Cell Host & Microbe
Article

The Ubiquitin Ligase Riplet Is Essential for RIG-I-Dependent Innate Immune Responses to RNA Virus Infection

Hiroyuki Oshiumi,[1,*] Moeko Miyashita,[1] Naokazu Inoue,[2] Masaru Okabe,[2] Misako Matsumoto,[1] and Tsukasa Seya[1]
[1]Department of Microbiology and Immunology, Graduate School of Medicine, Hokkaido University, Kita-15, Nishi-7, Kita-ku Sapporo 060-8638, Japan
[2]Research Institute for Microbial Diseases, Osaka University, 3-1 Yamadaoka, Suita, Osaka 565-0871, Japan
*Correspondence: oshiumi@med.hokudai.ac.jp
DOI 10.1016/j.chom.2010.11.008

SUMMARY

RNA virus infection is recognized by the RIG-I-like receptors RIG-I and MDA5, which induce antiviral responses including the production of type I interferons (IFNs) and proinflammatory cytokines. RIG-I is regulated by Lys63-linked polyubiquitination, and three E3 ubiquitin ligases, RNF125, TRIM25, and Riplet, are reported to target RIG-I for ubiquitination. To examine the importance of Riplet in vivo, we generated Riplet-deficient mice. Fibroblasts, macrophages, and conventional dendritic cells from Riplet-deficient animals were defective for the production of IFN and other cytokines in response to infection with several RNA viruses. However, Riplet was dispensable for the production of IFN in response to B-DNA and DNA virus infection. Riplet deficiency abolished RIG-I activation during RNA virus infection, and the mutant mice were more susceptible to vesicular stomatitis virus infection than wild-type mice. These data indicate that Riplet is essential for regulating RIG-I-mediated innate immune response against RNA virus infection in vivo.

INTRODUCTION

RNA virus infection is initially recognized by RIG-I-like receptors, RIG-I and MDA5, which induce antiviral responses such as the production of type I interferons (IFNs) and proinflammatory cytokines (Yoneyama and Fujita, 2009; Takeuchi and Akira, 2010). Analyses of RIG-I and MDA5 knockout mice showed that RIG-I is essential for type I IFN production by mouse embryonic fibroblasts (MEFs), conventional dendritic cells (cDCs), and macrophages (Mfs) in response to RNA viruses such as vesicular stomatitis virus (VSV), influenza A virus (Flu), hepatitis C virus (HCV), Sendai virus (SeV), and Japanese encephalitis virus (JEV). MDA5 is critical in picornavirus infection (Kato et al., 2006; Saito et al., 2007). However, in plasmacytoid DCs (pDCs), loss of RIG-I has no effect on viral induction of IFNs, and TLR7 and MyD88 are required for inducing immune responses in these cells (Diebold et al., 2004; Kato et al., 2005; Kumar et al., 2006; Sun et al., 2006).

RIG-I consists of two N-terminal CARDs, a central DExD/H helicase domain, and a C-terminal repressor domain (CTD) (Yoneyama et al., 2004). Before viral infection, CTD of RIG-I suppresses N-terminal CARDs (Saito et al., 2007). When the CTD of RIG-I recognizes the 5′ triphosphate-double-stranded (ds) viral RNA, the conformation of the RIG-I protein changes, and the N-terminal CARD triggers interaction with its downstream partner IPS-1 (Hornung et al., 2006; Pichlmair et al., 2006; Saito et al., 2007; Cui et al., 2008; Takahasi et al., 2008; Rehwinkel et al., 2010). IPS-1 contains an N-terminal CARD that interacts with the tandem CARDs of RIG-I and a C-terminal transmembrane domain that localizes it to the mitochondrial outer membrane (Kawai et al., 2005; Meylan et al., 2005; Seth et al., 2005; Xu et al., 2005). IPS-1 activates TBK1 kinase, which mediates phosphorylation of IRF-3, leading to its dimerization and translocation into the nucleus (Kumar et al., 2006; Sun et al., 2006). The IRF-3 dimers, NF-κB, and AP-1 transcription factors activate type I IFN transcription (Honda et al., 2005). The secreted type I IFNs activates the IFNAR, which leads to phosphorylation and nuclear translocation of STAT1 (Akira et al., 2006; Honda et al., 2006).

RIG-I is regulated by ubiquitination. Three E3 ubiquitin ligases, RNF125, TRIM25, and Riplet, target RIG-I (Arimoto et al., 2007; Gack et al., 2007; Oshiumi et al., 2009). RNF125 functions as a negative regulator for RIG-I signaling and mediates Lys48-linked polyubiquitination of RIG-I, leading to protein degradation by the proteasome (Arimoto et al., 2007). On the other hand, TRIM25 and Riplet function as positive regulators for the signaling. TRIM25 mediates Lys63-linked polyubiquitination at Lys172 of RIG-I CARDs (Gack et al., 2007). Lys63-linked polyubiquitination induces interaction between RIG-I and IPS-1 CARDs, leading to the activation of signaling (Gack et al., 2007, 2008). However, there are several reports that describe other models. First, Zeng et al. developed an in vitro reconstitution system of the RIG-I pathway (Zeng et al., 2010). Using this system, they showed that Lys172 of RIG-I CARDs is required for binding to the Lys63-linked polyubiquitin chain (Zeng et al., 2010). They postulated that polyubiquitin binding and not ubiquitin modification is required for RIG-I activation (Zeng et al., 2010). In their model, unanchored polyubiquitin chains are responsible for RIG-I activation. However, they did not rule out the possibility that ubiquitination of some signaling proteins may contribute to RIG-I activation (Zeng et al., 2010). Second, Fujita T and his colleagues reported that residue 172 of mouse RIG-I is not Lys but Gln and human RIG-I K172R mutant was normally activated by SeV infection in RIG-I KO MEFs (Shigemoto et al., 2009).

The third ubiquitin ligase, Riplet, mediates Lys63-linked polyubiquitination of RIG-I CTD and CARDs (Gao et al., 2009; Oshiumi et al., 2009). This polyubiquitination promotes RIG-I activation and its antiviral activity in human cells (Horner and Gale, 2009; Nakhaei et al., 2009; Takeuchi and Akira, 2010; Yoneyama and Fujita, 2010); however, in vivo evidence is absent. Type I IFNs are mainly produced by DCs or Mf in vivo, and RIG-I is essential for type I IFN production in cDC and Mf (Kato et al., 2005; Sun et al., 2006; Kumagai et al., 2007). The role of Riplet in these cells also has not yet been examined. Both TRIM25 and Riplet proteins mediate Lys63-linked polyubiquitination of RIG-I, and thus Gao et al. suggested that Riplet may be a complementary factor of TRIM25 for RIG-I activation (Gao et al., 2009). Therefore, it is not known whether Riplet is essential for RIG-I activation. To address these issues, we generated Riplet knockout mice. Our analysis revealed that Riplet is essential for the RIG-I activation and innate immune responses against viral infection in vivo.

RESULTS

Ubiquitous Expression of Riplet mRNA

First, we examined mouse Riplet mRNA expression by quantitative PCR (qPCR), and found it to be ubiquitously expressed in various tissues, MEFs, bone marrow-derived DCs (BM-DCs), and Mf (BM-Mf) (Figure 1A, left panel). Furthermore, we have previously shown that human Riplet mRNA is expressed in various tissues. When we examined the expression of Riplet mRNA in human DCs, it was observed in human DCs as in HeLa cells (Figure 1A, right panel). These data indicate that Riplet is expressed in various tissues and cells that are able to produce type I IFNs.

Generation of Riplet-Deficient Mice

Previously, we have shown that Riplet is a positive regulator for RIG-I-mediated signaling, and it mediates Lys63-linked polyubiquitination of RIG-I. However, the functional role of Riplet in vivo remains unclear. To investigate the role of Riplet in vivo, we generated Riplet-deficient (*Riplet*$^{-/-}$) mice by homologous recombination of embryonic stem cells (ESCs) (Figure 1B). We confirmed the target disruption of Riplet without deletion outside the targeted region (Figure 1C, and see Figures S1A and S1B available online). Riplet mRNA expression was abolished in *Riplet*$^{-/-}$ cells (Figures 1E and 1F), and the knockout of Riplet did not affect the expression of other genes, such as RIG-I, MDA5, IPS-1, TICAM-1, TLR3, and TRIM25, which are involved in type I IFN production (Figure 1F). The mutant mice were born at the Mendelian ratio from *Riplet*$^{+/-}$ parents (Figure 1D), and they developed and bred normally. These mice displayed no apparent abnormalities up to 7 months of age. Mutations in the human Riplet/RNF135 gene cause the overgrowth syndrome (Douglas et al., 2007). We did not observe any overgrowth phenotypes in *Riplet*$^{+/-}$ and *Riplet*$^{-/-}$ mice. Next, we examined the composition of CD4-, CD8-, CD11c-, and/or PDCA1-positive cells in the spleen, and found no difference between wild-type and *Riplet*$^{-/-}$ mice (Figures S1C and S1D). Induction of cDC from BM in the presence of GM-CSF was also normal in *Riplet*$^{-/-}$ mice (Figure S1E). Therefore, the mouse Riplet gene is dispensable for development.

Riplet$^{-/-}$ Embryonic Fibroblasts Are Defective in Innate Immune Responses against RNA Viruses

Riplet is a positive regulator for RIG-I-mediated signaling. In mouse fibroblast, VSV and Flu are mainly recognized by RIG-I (Kato et al., 2006). Furthermore HCV 3′UTR RNA is also recognized by RIG-I (Saito et al., 2008). Therefore, we first examined the expression of type I IFNs, IFN-inducible gene IP-10, and Ccl5 in MEFs after HCV 3′UTR dsRNA transfection or infection with VSV or Flu. The induction of mRNA of IFN-α2, -β, IP-10, and Ccl5 in response to VSV or Flu was abrogated in *Riplet*$^{-/-}$ MEFs (Figures 2A–2D). In addition, transfection of low concentration of HCV 3′UTR dsRNA (0.05–0.2 μg/well) also failed to upregulate IFN-α2, -β, and IFN-inducible genes in *Riplet*$^{-/-}$ MEFs (Figures 2A–2D).

Single-stranded (ss) RNA, which is synthesized by T7 RNA polymerase in vitro, induced lower IFN-β expression than dsRNA (Figure S2A). The induction of IFN-β mRNA by HCV 3′UTR ssRNA was also abolished in *Riplet*$^{-/-}$ MEFs (Figure S2A). Although the induction of IFN-β mRNA in response to VSV infection was abrogated in *Riplet*$^{-/-}$ MEFs even at high (moi = 5) or low multiplicities of infection (moi = 0.2 or 1), the induction of IFN-β mRNA in response to high concentration of HCV dsRNA (0.8 μg/well) was detected in *Riplet*$^{-/-}$ MEFs (Figures S2C–S2K). Therefore, RIG-I does not require Riplet function in the presence of large amounts of naked viral RNA in the cytoplasmic region.

Recently, Onoguchi et al. reported that type III IFN, IFN-λ, induction was RIG-I dependent during viral infection (Onoguchi et al., 2007). The induction of IFN-λ mRNA in response to VSV was also abrogated in *Riplet*$^{-/-}$ MEFs (Figure S2B).

Next, we examined type I IFNs or IL-6 levels in culture supernatants after viral infection or HCV 3′UTR RNA transfection (low concentration condition). The production of IFN-α, -β, and IL-6 in culture supernatants was abrogated in *Riplet*$^{-/-}$ MEFs (Figures 3A–3C). Next, we analyzed the contribution of Riplet to the antiviral response. When MEFs were infected with VSV at various mois, cytopathic effects (CPEs) were more severe in *Riplet*$^{-/-}$ than in wild-type MEFs (Figure 3D). These results demonstrate that Riplet plays a critical role in the elimination of RNA virus infection by induction of IFN responses.

Riplet Is Dispensable for the Production of Type I IFN Induced by B-DNA and HSV-1 Infection

Cytoplasmic B-form double-stranded DNA (dsDNA) stimulates the cells to induce type I IFNs and IFN-inducible genes (Ishii et al., 2006). TBK1 is required for type I IFN induction by dsDNA (Ishii et al., 2008). Although immortalized MEFs require RIG-I for type I IFNs production by dsDNA stimulation, primary MEFs do not require IPS-1, which is a RIG-I adaptor, for type I IFNs production by dsDNA (Kumar et al., 2006; Chiu et al., 2009). We examined the expression of IFN-β and IP-10 mRNA by dsDNA stimulation in primary wild-type and *Riplet*$^{-/-}$ MEFs. IFN-β and IP-10 mRNA were detected in *Riplet*$^{-/-}$ MEFs by dsDNA transfection similar to that detected in wild-type MEFs (Figures 4A and 4B).

Next, we examined IFN-β mRNA expression during infection with DNA virus, HSV-1. Wild-type and *Riplet*$^{-/-}$ MEFs were infected with HSV-1, and IFN-β mRNA expression was examined by RT-qPCR. IFN-β expression in *Riplet*$^{-/-}$ MEFs was comparable to that in wild-type MEFs (Figure 4C). Taken together, these

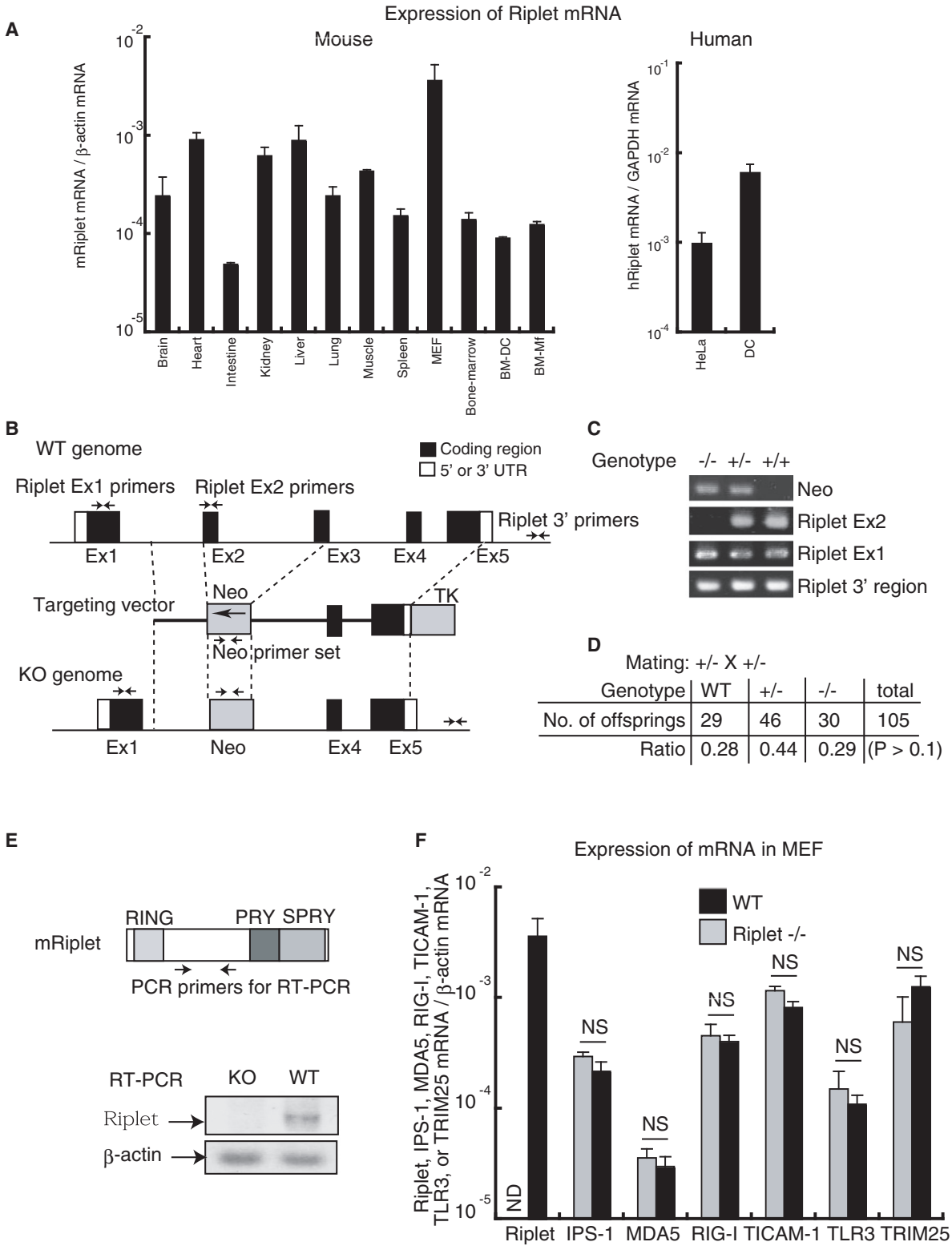

Figure 1. Targeted Disruption of the Murine Riplet Gene

(A) Riplet mRNA expression in mouse tissues and cells or human cells. RT-qPCR was performed to measure Riplet mRNA, and each sample was normalized to β-actin (mouse) or GAPDH (human). Data are shown as means ±SD and are representative of three independent experiments.

(B) Structure of the mouse Riplet gene, targeting vector, and disrupted gene. Closed boxes indicate the coding exon of Riplet, and hatched boxes indicate the Neo or TK gene coding region. The primer sets for PCR are shown by arrows.

data indicate that Riplet-dependent RIG-I activation is dispensable for type I IFN and IFN-inducible genes mRNA expression by cytoplasmic DNA in primary MEFs. This is consistent with previous studies reporting that the IPS-1-dependent pathway is dispensable for type I IFN production by cytoplasmic dsDNA stimulation (Kumar et al., 2006).

Riplet Is Essential for Triggering the RIG-I Signaling Pathway

We further examined the role of Riplet in RIG-I-mediated signaling during RNA virus infection. In RIG-I-mediated signaling, induction of type I IFNs and proinflammatory cytokines requires the activation of transcription factor IRF3. IRF3 is phosphorylated by TBK1 and IKK-ε. Phosphorylated IRF3 induces IFN-β gene expression. IFN-β produced subsequently stimulates the JAK-STAT pathway to amplify the responses. To determine the role of Riplet in signaling pathway activation, we analyzed IRF3 and STAT1 activations after VSV infection in *Riplet*$^{-/-}$ MEFs. VSV-induced dimerization of IRF3 and VSV- or Flu-induced pohsphorylation of STAT1 were abrogated in *Riplet*$^{-/-}$ MEFs (Figures 3E and 3F). These results demonstrate that Riplet is essential for activating the transcription factors that work early phase of RNA virus infection.

In the absence of viral infection, RIG-I CTD suppressed N-terminal CARDs (Saito et al., 2007). After viral infection, RIG-I CTD binds to viral RNA, leading to conformational changes (Saito et al., 2007). Later, RIG-I CARDs undergo TRIM25-mediated polyubiquitination and associate with IPS-1 CARD (Gack et al., 2007, 2008). When we tested the effect of Riplet on RIG-I activation, the full-length RIG-I protein with CTD failed to activate the IFN-β promoter in *Riplet*$^{-/-}$ MEFs (Figure 5A); however, promoter activation by the expression of RIG-I CARDs without CTD was normal in *Riplet*$^{-/-}$ MEFs (Figure 5B). These data indicate that Riplet is required for the activation of full-length RIG-I, but not for the activation of RIG-I CARDs without CTD. Next, we performed complementation assays. Immortalized *Riplet*$^{-/-}$ MEFs were transfected with an empty-, RIG-I-, or RIG-I-5KA mutant-expressing vector together with or without Riplet-expressing vector. The RIG-I-5KA mutant harbors mutations in five C-terminal Lys residues that are important for Riplet-mediated ubiquitination (Oshiumi et al., 2009). In the *Riplet*$^{-/-}$ cell line, RIG-I was not activated by HCV RNA stimulation, and Riplet expression led to the activation of wild-type RIG-I (Figure 5C). The deletion of the Riplet RING finger domain, which is the catalytic domain of ubiquitin ligase, abolished RIG-I activation (Figure 5D). Unlike wild-type RIG-I, Riplet expression failed to activate the RIG-I-5KA mutant protein (Figure 5C). The activations of wild-type and mutant RIG-I were correlated with its polyubiquitination (Figure S3A). Although the RNA binding activity was weakly reduced by the 5KA mutation, the pull-down assay showed that RIG-I-5KA mutant bound to dsRNA (Figure S3B). Next, we examined ligand-independent RIG-I activation by overexpression of Riplet. Overexpression of Riplet in HEK293 cells activated RIG-I in the absence of RIG-I ligand, such as viral RNA (Figure S3C). This ligand-independent activation of RIG-I by Riplet overexpression was also abolished by the 5KA mutation (Figure S3C). In addition, we examined the polyubiquitination of exogenously expressed RIG-I CTD fragment. Polyubiquitination of RIG-I CTD fragment was increased by overexpression of Riplet (Figure 5M), and was reduced by overexpression of the dominant-negative form of Riplet (Riplet DN) (Figure 5N). Polyubiquitination of RIG-I CTD fragment was not detected in Riplet-deficient cells (R3T cells); however, expression of Riplet led to polyubiquitination of RIG-I CTD fragment (Figure 5O). These data are consistent with our previous report (Oshiumi et al., 2009). Taken together, these data indicate that Riplet-dependent polyubiquitination of RIG-I is important for RIG-I activation.

Previously, we showed that Riplet is not involved in MDA5-mediated signaling. IFN-β promoter activation by MDA5 overexpression was normal in *Riplet*$^{-/-}$ MEFs (Figure 5E). Transfection of poly(I:C), which is recognized by MDA5, induced IFN-β, IL-6, and IP-10 expression in both wild-type and *Riplet*$^{-/-}$ MEFs (Figures 5F–5H). In addition, stimulation with lipopolysaccharide (LPS), which is a TLR4 ligand, normally induced expression of these cytokines in *Riplet*$^{-/-}$ MEFs (Figures 5I–5K). Furthermore, IL-6 production in culture medium in response to LPS was normal in *Riplet*$^{-/-}$ MEFs (Figure 5L). Taken together, these data indicate that Riplet is essential for the RIG-I-mediated type I IFN or IL-6 production upon viral infection in nonprofessional immune cells like fibroblasts, but is not required for MDA5- or TLR4-mediated signaling.

Riplet Is Required for Antiviral Innate Immune Responses in Conventional Dendritic Cells and Macrophages

We examined whether Riplet is required for the induction of type I IFN in DCs or Mf. DCs play a pivotal role in bridging innate and adaptive immune responses, and can be classified into cDCs and pDCs, the latter producing high levels of type I IFNs. Mfs also produce type I IFN. We induced cDCs from BM cells in the presence of GM-CSF (BM-DC). Twenty-four hours after VSV or Flu infection, cDCs of wild-type mice produced IFN-α, -β, and IL-6 (Figures 6A–6F). In contrast, the cDCs of *Riplet*$^{-/-}$ mice showed severely impaired IFN-α, -β, or IL-6 production during VSV or Flu infection (Figures 6A–6F). When the cDCs were stimulated with a TLR4 ligand, such as LPS, IFN-β or IL-6 production in *Riplet*$^{-/-}$ cDCs was almost normal (Figures S4A and S4B), indicating that Riplet is dispensable for LPS-induced cytokine production in cDCs.

Then we tested M-CSF-induced BM-Mf. Wild-type Mf produced IFN-α, -β, and IL-6 after VSV or Flu infection (Figures

(C) PCR of mouse tail. Genomic DNA was extracted from wild-type, *Riplet*$^{+/-}$, or *Riplet*$^{-/-}$ mice tails and PCR was performed using primers shown in (B).
(D) Genotype analyses of offspring from heterozygote intercrosses. Chi-square goodness-of-fit test indicated that deviation from Mendelian ratio was not statistically significant ($p > 0.1$).
(E) RT-PCR of MEFs. Total RNA from wild-type and *Riplet*$^{-/-}$ MEFs were extracted and subjected to RT-PCR to determine Riplet mRNA expression.
(F) Riplet, IPS-1 MDA5, RIG-I, TICAM-1, TLR3, and TRIM25 expression in MEFs. Total RNA from wild-type and *Riplet*$^{-/-}$ MEFs were extracted and subjected to RT-qPCR to determine mRNA expression. Expression of the indicated gene mRNA was normalized to β-actin mRNA expression. Data are shown as means ±SD and are representative of three independent experiments. "NS" indicates no statistically significant difference between the two samples.
See also Figure S1 and Table S1.

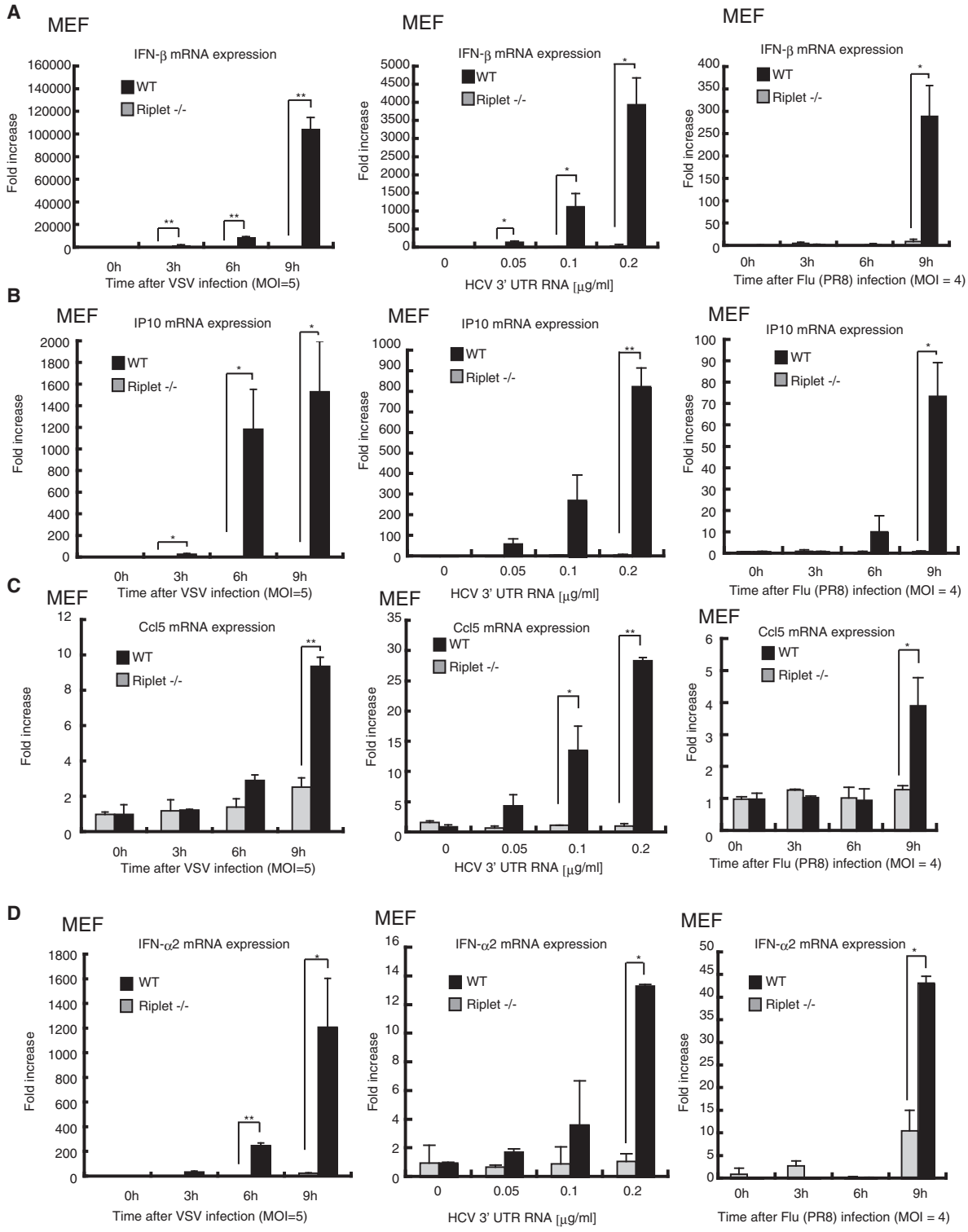

Figure 2. Abolished Responses to RNA Virus Infection in *Riplet*$^{-/-}$ Fibroblasts

Wild-type or *Riplet*$^{-/-}$ MEFs were infected with VSV or influenza A virus (Flu), and total RNA was extracted at the indicated times. Short HCV 3′UTR dsRNA was transfected into wild-type or *Riplet*$^{-/-}$ MEFs, and total RNA was extracted after 24 hr. Extracted RNA was subjected to RT-qPCR to determine IFN-β (A), IP10 (B), Ccl5 (C), or IFN-α2 (D) expression. Expression of each sample was normalized to β-actin mRNA expression. Data are shown as means ±SD and are representative of three independent experiments. *$p < 0.05$, **$p < 0.01$ (t test).

See also Figure S2 and Table S1.

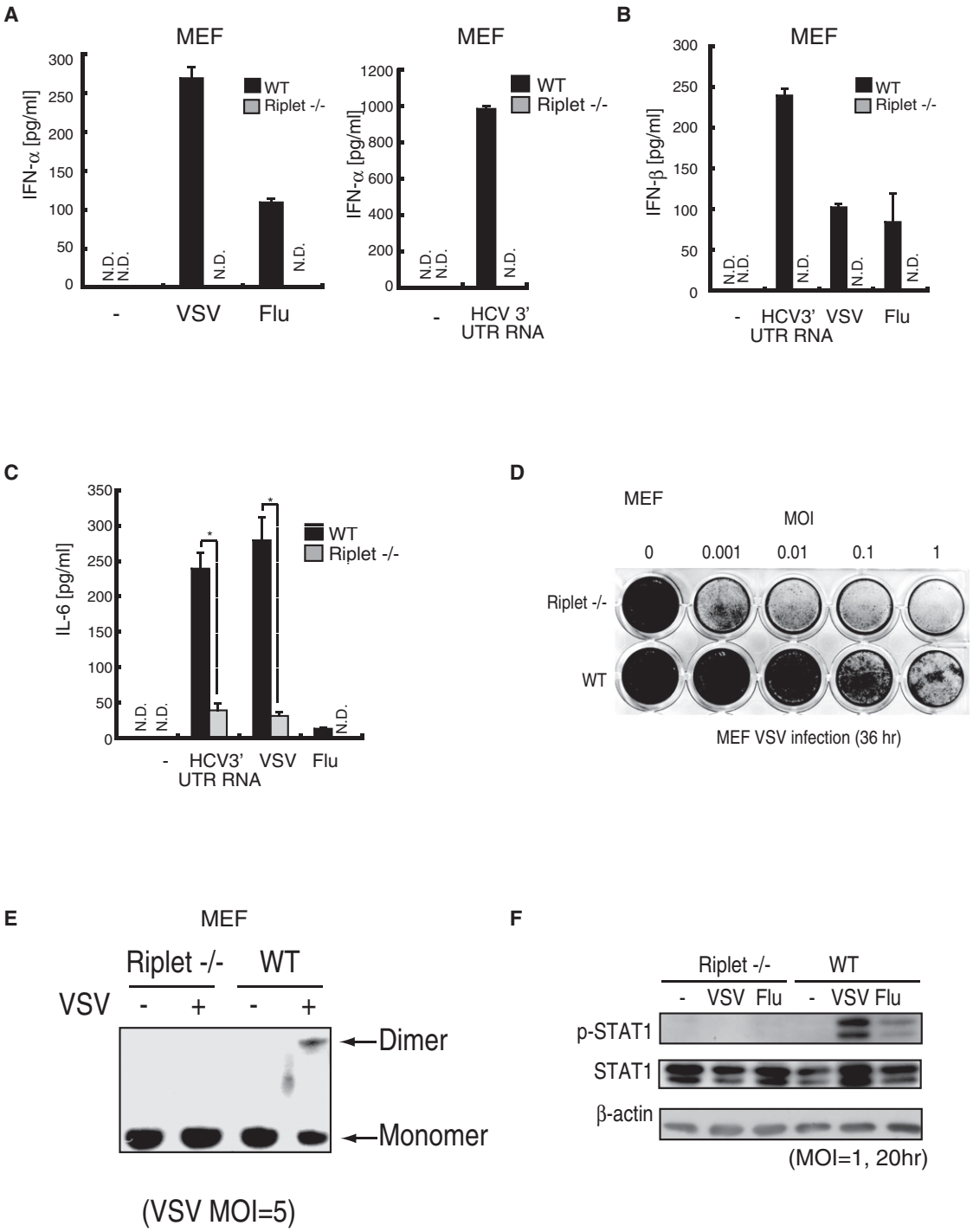

Figure 3. Role of Riplet in Antiviral Responses in Fibroblasts

(A–C) Wild-type or *Riplet*$^{-/-}$ MEFs were infected with VSV or Flu or transfected with short HCV 3′UTR dsRNA. Amounts of IFN-α (A), -β (B), and IL-6 (C) in culture supernatants were measured by ELISA after 24 hr. Data are shown as means ±SD and are representative of three independent experiments. *$p < 0.05$, **$p < 0.01$ (t test).

(D) Wild-type or *Riplet*$^{-/-}$ MEFs were infected with VSV at the indicated moi, and after 36 hr MEFs were fixed with formaldehyde and stained with crystal violet.

(E) Wild-type or *Riplet*$^{-/-}$ MEFs were infected with VSV at moi = 5, and after 9 hr cell lysates were prepared and analyzed by native PAGE. IRF-3 proteins were stained with anti-IRF3 antibody.

(F) Wild-type or *Riplet*$^{-/-}$ MEFs were infected with VSV or Flu at moi = 1, and after 20 hr cell lysates were prepared. The samples were analyzed by SDS-PAGE and western blotting. They were stained with anti-STAT1, phospho-STAT1, or β-actin antibodies.

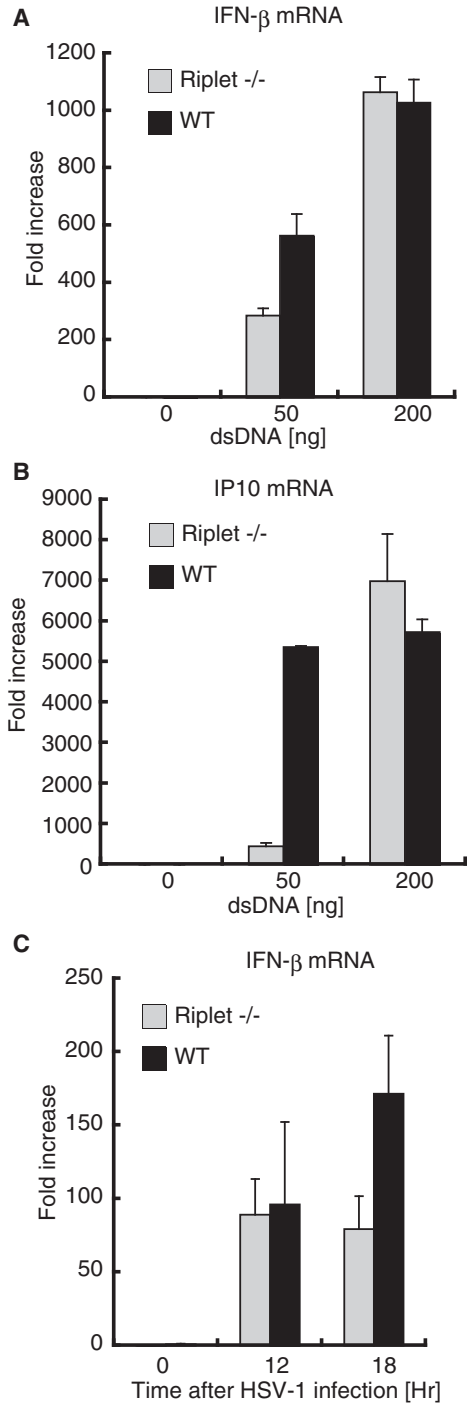

Figure 4. Role of Riplet in Type I IFN Production Induced by Cytoplasmic dsDNA

(A and B) Wild-type and *Riplet*$^{-/-}$ MEFs were transfected with the indicated amounts of dsDNA (Salomon sperm DNA) using the Lipofectamine 2000 reagent. Nine hours after the transfection, IFN-β (A) and IP-10 (B) mRNA expression was determined by RT-qPCR. Data are shown as means ±SD and are representative of three independent experiments.

(C) Wild-type and *Riplet*$^{-/-}$ MEFs were infected with HSV-1 at moi = 4, and IFN-β mRNA expression at the indicated times was examined by RT-qPCR. Data are shown as means ±SD and are representative of three independent experiments.

6A–6F). Similar to cDCs, cytokine production was reduced in Riplet knockout mice (Figures 6A–6F). Peritoneal Mf were isolated from wild-type and *Riplet*$^{-/-}$ mice. Knockout of Riplet reduced type I IFN production from peritoneal Mfs during VSV infection (Figures S4C and S4D).

We next generated Flt3L-induced DCs (Flt3L-DCs), which contain pDCs. Akira and his colleagues previously showed that the knockout of RIG-I or IPS-1 does not reduce type I IFN and IL-6 production by Flt3L-DCs, because RIG-I is dispensable for cytokine production in pDCs (Kato et al., 2005). The Flt3L-DCs of *Riplet*$^{-/-}$ mice produced normal amounts of IFN-a, -β, and IL-6 during Flu infection (Figures 6A–6F). This is consistent with the notion that Riplet is essential for the RIG-I-mediated type I IFNs and IL-6 production. Although the IFN-α levels in the culture medium after VSV infection were comparable with those in wild-type and *Riplet*$^{-/-}$ mice, Flt3L-DCs of *Riplet*$^{-/-}$ mice produced less IL-6 compared with that produced by wild-type mice through an unknown mechanism (Figure 6C).

Next, we examined type I IFN production during SeV infection. SeV infection induced IFN-α and -β productions from wild-type BM-DC, and the knockout of Riplet reduced IFN-α and -β productions from BM-DC (Figures S4E–S4J). Wild-type Flt3L-DC produced IFN-α after SeV infection, and the knockout of Riplet did not reduce IFN- α production from Flt3L-DC (Figures S4E–S4J).

Riplet Is Essential for Antiviral Immune Defense In Vivo

To investigate the role of Riplet in antiviral responses in vivo, wild-type and *Riplet*$^{-/-}$ mice were injected intraperitoneally with wild-type VSV, and sera were collected to measure type I IFN and IL-6 levels. IFN-α, -β, and IL-6 levels in sera were markedly reduced in *Riplet*$^{-/-}$ mice compared to in wild-type mice (Figures 7A and 7B, and Figure S5A). Next, wild-type and *Riplet*$^{-/-}$ mice were intranasally infected with VSV, and type I IFN levels in their sera were measured. At early time points, IFN-α and -β production was reduced in *Riplet*$^{-/-}$ mice compared to wild-type mice (Figures 7C and 7D); however, cytokine levels were comparable at later time points (Figures S5B and S5C). Previously, Ishikawa et al. observed that the knockout of STING gene, which is involved in RIG-I-dependent signaling, leads to reduction of type I IFN at early time points and relatively less reduction at later time points (Ishikawa and Barber, 2008; Ishikawa et al., 2009).

To determine if Riplet deficiency affects the survival of mice after VSV infection, the mice were intranasally infected with VSV, and their survival was monitored. Wild-type mice survived VSV infection; however, *Riplet*$^{-/-}$ mice were susceptible to VSV infection (Figure 7E). The viral titer in *Riplet*$^{-/-}$ mice brains 7 days after infection was higher than in wild-type mice (Figure 7F). These data indicate that Riplet plays a key role in the host defenses against VSV infection in vivo, and type I IFN production at early time points is important for host defenses.

DISCUSSION

In this study, we presented genetic evidence that Riplet is indispensable for antiviral responses in MEFs, BM-Mf, and BM-DCs, but not in Flt3L-DCs. The cell-type-specific requirement of Riplet

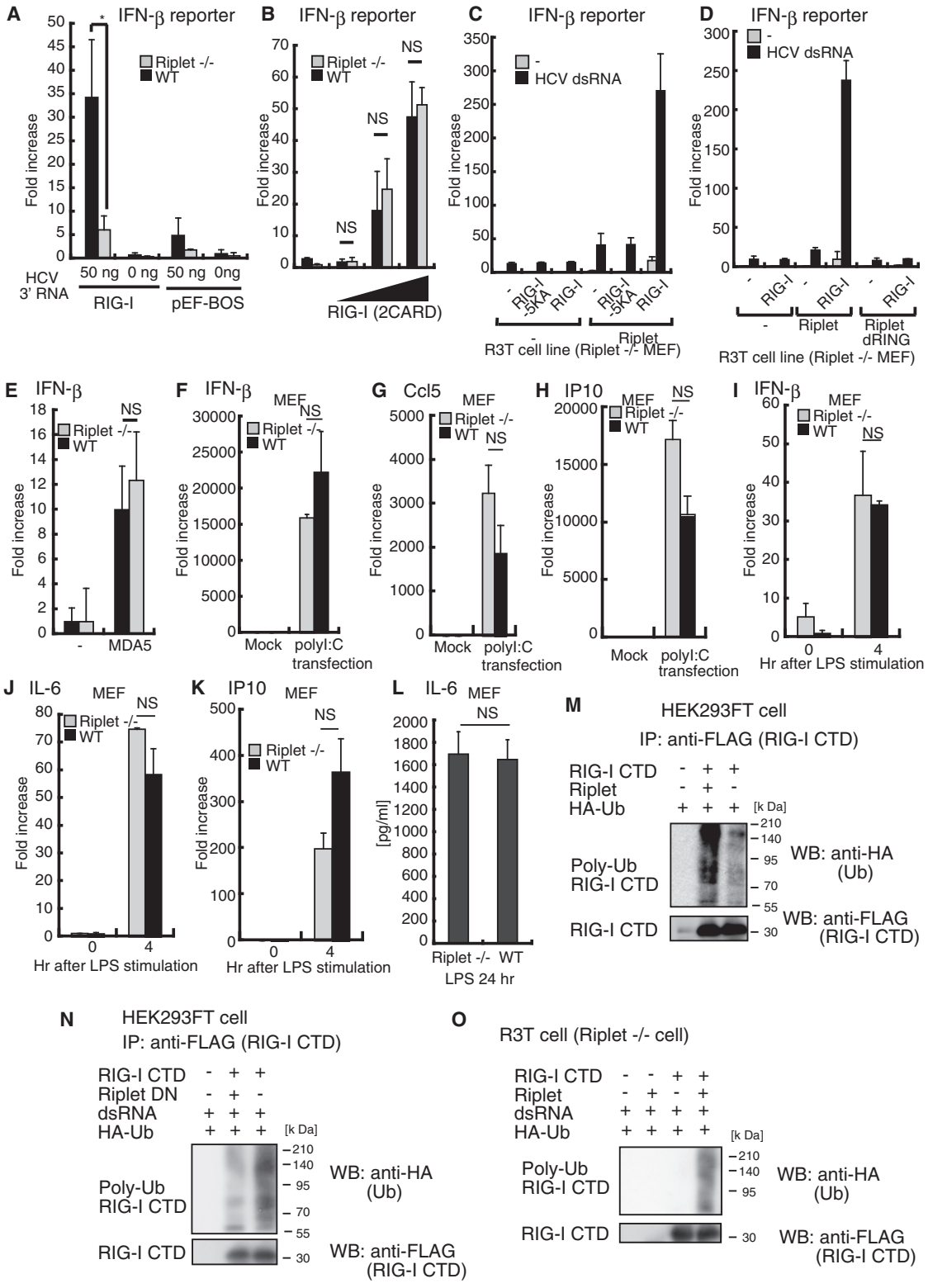

Figure 5. Role of Riplet in the RIG-I-Dependent Pathway

(A) Expression vector of full-length RIG-I and reporter plasmids were transfected into wild-type or *Riplet*$^{-/-}$ MEFs with or without HCV 3′UTR short dsRNA, and after 24 hr IFN-β promoter activation was examined by reporter gene assay. Data are shown as means ±SD and are representative of three independent experiments. *$p < 0.05$ (t test).

is similar to that of RIG-I. Previously, we showed that Riplet binds to RIG-I and mediates Lys63-linked polyubiquitination of RIG-I (Oshiumi et al., 2009). Genetic evidence in this study revealed that Riplet function is essential for RIG-I-dependent type I IFN production. Knockout of Riplet reduced type I IFN production in vivo during the early phase of VSV infection, and *Riplet*$^{-/-}$ mice were susceptible to VSV infection. Taken together, our results provide genetic evidence that Riplet is essential for RIG-I-dependent antiviral immune response in vivo. Most *RIG-I*$^{-/-}$ embryos were lethal at embryonic days 12.5–14.0 in some strain backgrounds (Kato et al., 2005). However, we could not observe any developmental defect in Riplet knockout mice as far as we examined.

Previously, Chen and his colleagues independently isolated Riplet and named it REUL (Gao et al., 2009). They reported that REUL/Riplet binds to RIG-I CARDs but not to CTD (Gao et al., 2009). Furthermore, they reported that REUL/Riplet mediates Lys63-linked polyubiquitination of Lys172 of RIG-I CARDs in a manner similar to TRIM25 (Gack et al., 2007; Gao et al., 2009). Although they did not show any expression profile data for Riplet and TRIM25, they mentioned that TRIM25 and Riplet have different distribution patterns, and thus hypothesized that REUL/Riplet is a complementary factor of TRIM25 and is required for RIG-I activation in cells that do not express TRIM25 (Gao et al., 2009). However, our genetic evidence is not consistent with their hypothesis, because Riplet is essential for RIG-I activation in MEFs that express TRIM25. Previously, Gack et al. showed that knockout of TRIM25 alone abolished RIG-I activation in MEFs (Gack et al., 2007). Therefore, null mutation in either Riplet or TRIM25 abolishes RIG-I activation. This genetic evidence indicates that Riplet can mediate polyubiquitination of RIG-I Lys residues that are not ubiquitinated by TRIM25. This means that Riplet functions differently than TRIM25 in RIG-I activation.

We isolated Riplet cDNA by yeast two-hybrid screening using the C-terminal region of RIG-I (Oshiumi et al., 2009). Because the yeast genome does not encode RIG-I, the interaction indicates the direct binding of Riplet to the RIG-I C-terminal region. The interaction between RIG-I CTD and Riplet has also been confirmed by immunoprecipitation assays in human cells (Oshiumi et al., 2009). Moreover, we have shown that Riplet expression leads to Lys63-linked polyubiquitination of RIG-I CTD (Oshiumi et al., 2009). Recently, Zheng et al. showed that RIG-I CARDs has the ability to bind to polyubiquitin chains (Zeng et al., 2010). We have carefully detected Riplet-mediated polyubiquitination of RIG-I C-terminal region without CARDs, under high-salt conditions, in which many protein-protein interactions were abolished (Oshiumi et al., 2009). Therefore, we proposed the hypothesis that Riplet mediates Lys63-linked polyubiquitination of RIG-I CTD (Oshiumi et al., 2009). This model can explain the genetic evidence that Riplet is essential for RIG-I activation in MEFs that express TRIM25. Gack et al. showed that K172R mutation alone caused near-complete loss of ubiquitination of the human RIG-I CARDs (Gack et al., 2007). Because residue 172 of mouse RIG-I is not Lys but Gln (Shigemoto et al., 2009), Riplet/Reul does not ubiquitinate residue 172 of mouse RIG-I. Based on the previous studies and our current data, we prefer the interpretation that Riplet activates RIG-I through polyubiquitination of RIG-I CTD. However, this interpretation does not exclude the possibility that Riplet ubiquitinates both CTD and CARDs of RIG-I (Gao et al., 2009; Oshiumi et al., 2009).

Previously, we showed that Lys849, -851, -888, -907, and -909 are critical residues in Riplet-mediated RIG-I CTD ubiquitination (Oshiumi et al., 2009). These five Lys residuse are close to the dsRNA binding sites of RIG-I CTD (Takahasi et al., 2008), and the 5KA mutation weakly reduced RNA binding activity of RIG-I. Therefore, it is possible that the 5KA mutation abrogate activation and polyubiquitination of RIG-I by reducing RNA biding activity of RIG-I. However, this possibility is weakened by following observations. First, the 5KA mutation caused near-complete loss of RIG-I activation, but the RIG-I-5KA mutant protein still possessed RNA binding activity. Second, overexpression of Riplet led to RIG-I activation in the absence of dsRNA in HEK293 cells, and this ligand-independent activation of RIG-I

(B) Expression vector for the two RIG-I N-terminal CARDs were transfected into wild-type or *Riplet*$^{-/-}$ MEFs together with reporter plasmids, and IFN-β promoter activation was examined by the reporter gene assay. Data are shown as means ±SD and are representative of three independent experiments. "NS" indicates not statistically significant.

(C) Empty, wild-type RIG-I-, or RIG-I-5KA mutant-expressing vectors were transfected into the *Riplet*$^{-/-}$ MEF cell line together with or without the Riplet-expressing vector. Cells were stimulated with HCV 3′UTR short dsRNA, and reporter gene assay was performed as described in (A).

(D) Empty or wild-type RIG-I-expressing vectors were transfected into the *Riplet*$^{-/-}$ MEF cell line together with empty, wild-type Riplet, or Riplet mutant (Riplet dRING)-expressing vector. Cells were stimulated with HCV 3′UTR short dsRNA, and the reporter gene assay was performed as described in (A).

(E) Empty or MDA5-expressing vectors was transfected into wild-type or *Riplet*$^{-/-}$ MEFs together with reporter plasmids, and after 24 hr IFN-β promoter activation was examined by the reporter gene assay.

(F–H) Of poly(I:C), 0.8 μg was transfected into wild-type or *Riplet*$^{-/-}$ MEFs. Twenty-four hours after transfection, total RNA was extracted from MEFs and subjected to RT-qPCR to determine IFN-β (F), Ccl5 (G), and IP10 (H) expression. Expression in each sample was normalized to the β-actin mRNA expression.

(I–K) Wild-type or *Riplet*$^{-/-}$ MEFs were stimulated with 1 μg of LPS. Total RNA was extracted at the indicated times and subjected to RT-qPCR analysis for of IFN-β (I), IL-6 (J), or IP-10 (K) expression.

(L) Wild-type or *Riplet*$^{-/-}$ MEFs were stimulated with LPS, and after 24 hr the amount of IL-6 in culture supernatants was measured by ELISA.

(M) HEK293FT cells were transfected with Riplet, FLAG-tagged RIG-I-CTD, and HA-tagged ubiquitin (HA-Ub) expression vectors. Twenty-four hours after transfection, cell lysates were extracted and immunoprecipitation was carried out with anti-FLAG antibody as previously described (Oshiumi et al., 2009). The samples were analyzed by SDS-PAGE, and western blotting was performed using anti-HA polyclonal antibody (Ub) and anit-Flag M2 monoclonal antibody (RIG-I-CTD). The plasmids are described previously (Oshiumi et al., 2009).

(N) Expression vector of dominant negative form of Riplet (Riplet DN) was transfected into HEK293FT cells together with expression vector of FLAG-tagged RIG-I CTD and HA-tagged ubiquitin. Cells were stimulated with dsRNA. Ubiquitination of RIG-I CTD was detected as in (M).

(O) R3T cells were transfected with Riplet, FLAG-tagged RIG-I-CTD, and HA-tagged ubiquitin (HA-Ub) expression vectors. Cells were stimulated with dsRNA. Ubiquitination of RIG-I-CTD was detected as in (M).

See also Figure S3.

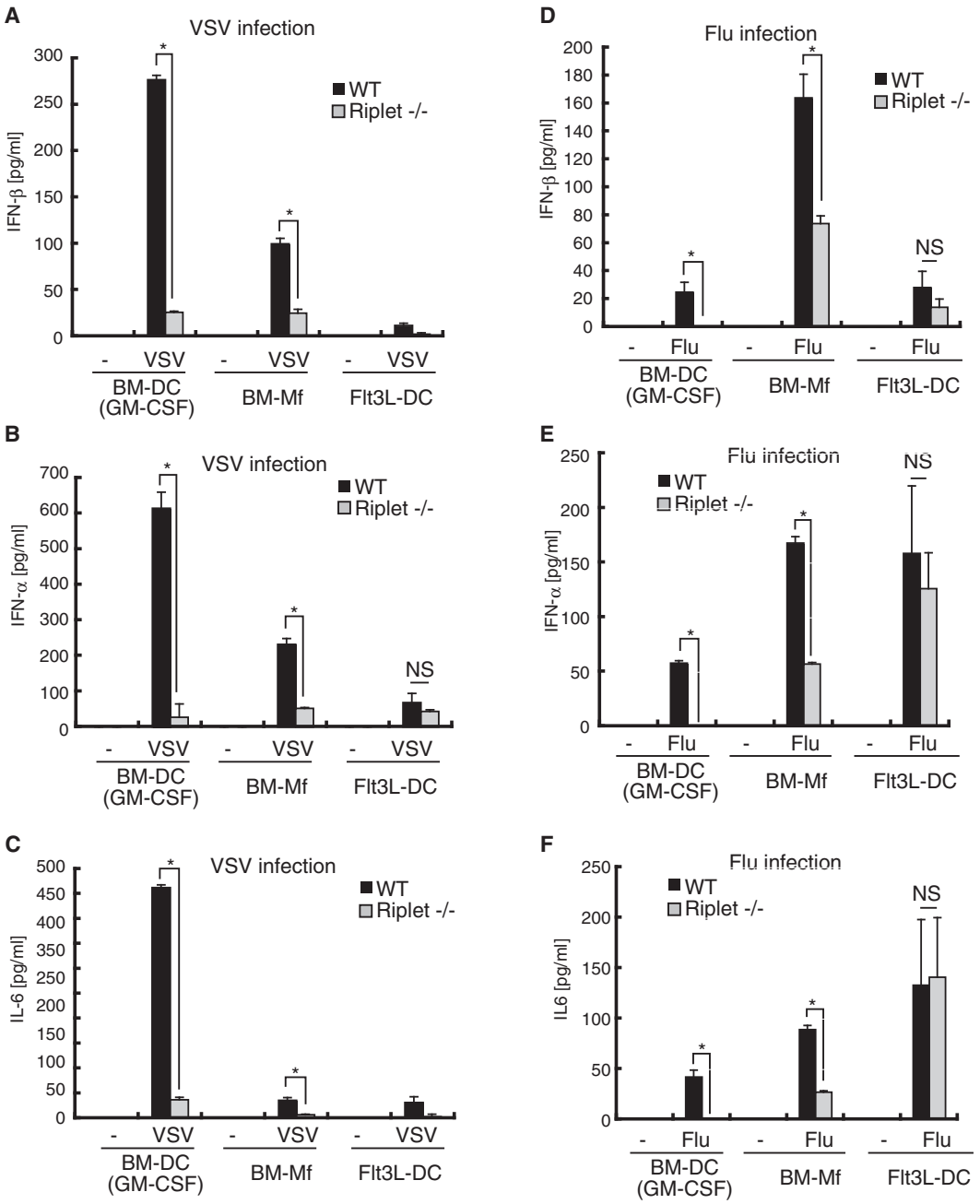

Figure 6. Role of Riplet in Responses to VSV or Flu Infection in Bone Marrow-Derived Cells

GM-DCs, BM-Mf, or Flt3L-DCs were induced from BM-derived cells in the presence of GM-CSF, M-CSF, or Flt3L and infected with VSV or influenza A virus at moi = 1. Twenty-four hours after viral infection, amounts of IFN-β (A and D), -α (B and E), and IL-6 (C and F) in culture supernatants were measured by ELISA. Data are shown as means ±SD and are representative of two independent experiments. *$p < 0.05$ (Student's t test). NS indicates not statistically significant.
See also Figure S4.

by overexpression of Riplet was also abolished by the 5KA mutation. These data support our model. However, we do not exclude the possibility that other Lys residues of RIG-I are ubiquitinated by Riplet, because we have not yet directly detected polyubiquitinated residues of RIG-I CTD by mass spectrometory analysis. Further in vitro studies are required to determine the polyubiquitination sites and to reveal precise RIG-I regulatory mechanisms by Riplet-mediated Lys63-linked polyubiquitation.

In general, E3 ubiquitin ligase targets several types of proteins. Therefore, it is possible that Riplet targets other proteins. Previous work has shown that Riplet binds to the Trk-fused gene (TFG) protein (Suzuki et al., 2001). The TFG protein interacts with TANK and NEMO, which are involved in the NF-κB pathway (Miranda et al., 2006). Although NEMO is involved in IPS-1-mediated signaling, RIG-I CARDs- or MDA5-mediated signaling was normal in *Riplet*$^{-/-}$ MEFs. Therefore, interaction between Riplet

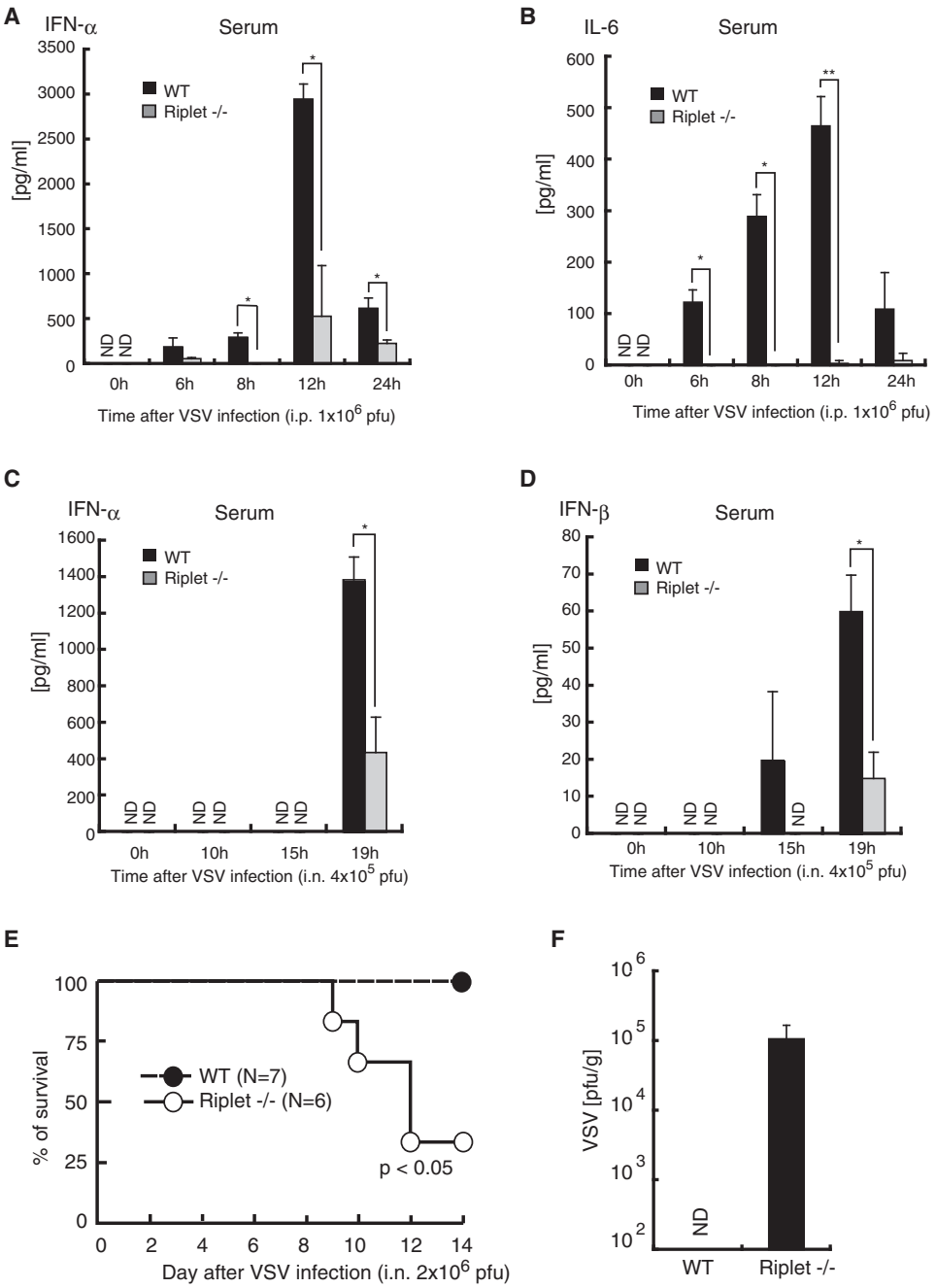

Figure 7. Role of Riplet in Antiviral Responses In Vivo

(A and B) Wild-type or *Riplet*$^{-/-}$ mice were injected intraperitoneally with 1 × 10^6 pfu of VSV. Amounts of IFN-α (A) and IL-6 (B) in mouse serum were measured by ELISA. Data are shown as mean ±SD of samples obtained from three wild-type and three Riplet −/− mice at each time point. *p < 0.05 (Student's t test). "ND" indicates not detected.

(C and D) Wild-type and *Riplet*$^{-/-}$ mice were infected intranasally with 4 × 10^5 pfu of VSV. Amounts of IFN-α (C) and IFN-β (D) in mouse serum were measured by ELISA.

(E) Wild-type and *Riplet*$^{-/-}$ mice were infected intranasally with 2 × 10^6 pfu of VSV and mice mortality was observed for 14 days (*p < 0.05 between wild-type and *Riplet*$^{-/-}$ mice, log rank test).

(F) Wild-type and *Riplet*$^{-/-}$ mice were infected intranasally with 2 × 10^6 pfu of VSV, and sacrificed for their tissues on day 7 after infection. Titers in brain were determined by the plaque assay. Viral titers in brains of wild-type mice were below 100 pfu/g, and thus not detected (ND). Data are shown as means ±SD (n = 3). See also Figure S5.

and TFG protein is not required for RIG-I-mediated signaling. However, since TFG is involved in tumorigenesis (Miranda et al., 2006), Riplet may be involved in human tumorigenesis.

Several viral proteins inhibit RIG-I-mediated signaling. For example, Flu NS1 inhibits TRIM25 and HCV NS3/4A cleaves IPS-1 (Meylan et al., 2005; Gack et al., 2009). Therefore, Riplet may be inhibited by viral proteins. Indeed, our pilot study indicated that the Riplet protein is disrupted in human hepatocyte cell lines carrying a full-length HCV replicon. RIG-I is involved in innate immune responses against various viruses. In this study, we showed that Riplet is required for innate immune responses against VSV, Flu, and SeV. Therefore, Riplet is also expected to be involved in innate immune responses against other viruses that are recognized by RIG-I.

EXPERIMENTAL PROCEDURES

Generation of Riplet-Deficient Mice

The Riplet gene was amplified by PCR using genomic DNA extracted from ESCs by PCR. The targeting vector was constructed by replacing the second and third exons with a neomycine-resistance gene cassette (Neo), and a herpes simplex virus thymidine kinase (HSV-TK) driven by PGK promoter was inserted into the genomic fragment for negative selection. After the targeting vector was transfected into 129/Sv mice-derived ESCs, G418 and gancyclovir doubly resistant colonies were selected and screened by PCR. The targeted cell line was injected in C57BL/6 blastocysts, resulting in the birth of male chimeric mice. These mice were then crossed with 129/Sv mice to obtain heterozygous mutants. The heterozygous mutants were intercrossed to obtain homozygous *Riplet*$^{-/-}$ mice.

Cells, Viruses, and Reagents

Wild-type and *Riplet*$^{-/-}$ MEFs were prepared from day 12.5–13.5 embryos. *Riplet*$^{-/-}$ MEFs were immortalized with large T antigen and named R3T cell line. BM cells were prepared from 5- to 10-week-old mice. VSV Indiana strain was provided by A. Takada (Hokkaido University). VSV was amplified using Vero cells and the viral titer was determined by the plaque assay. Flu (PR8 strain) and SeV (HVJ strain) was provided by Y. Sakoda (Hokkaido University). HSV-1 strain was provided by K. Kondo (The JIKEI University). Anti-mouse IRF3 antibody was purchased from Zymed. Anti-phospho-STAT1 antibody was purchased from Cell Signaling and anti-STAT1 antibody from Santa Cruz. Salomon sperm dsDNA was purchased from Invitrogen. To determine the viral titer in the brain, the mice were sacrificed, and the brain was aseptically removed and frozen at −80°C. The brain was homogenized in 1 ml of PBS on ice, and the titer was determined by plaque assay.

Preparation of Viral Double-Stranded RNA

cDNA of the HCV 3′UTR region was amplified from total RNA of the HCV genotype 1b full-length replicon using primers HCV-F1 and HCV-R1, and then cloned in the pGEM-T Easy Vector. The primer set sequences were HCV-F1, CTCCAGGTGAGATCAATAGG; and HCV-R1, CGTGACTAGGGCTAAGATGG. RNA was synthesized using T7 and SP6 RNA polymerases. Template DNA was digested by DNase I, and RNA was purified using TRIZOL (Invitrogen) according to manufacturer's instructions.

Quantitative PCR

For qPCR, total RNA was extracted with TRIZOL (Invitrogen) and 0.5 μg of RNA was reverse-transcribed using the High Capacity cDNA Transcription Kit (ABI) with random primers according to the manufacturer's instructions. qPCR was performed using the Step One Real-Time PCR system (ABI). Primer sequences used for qPCR are listed in Table S1.

Measurement of Cytokines

In brief, 5 × 10^5 cells in a 24-well plate were either infected with VSV or Flu, stimulated with LPS, or transfected with HCV 3′UTR dsRNA or poly(I:C). Twenty-four hours after infection, stimulation, or transfection, culture supernatants were collected and analyzed for IFN-α, -β, and IL-6 production by ELISA. Cytokine levels were measured in mouse serum obtained from the mouse tail vein. ELISA kits for mouse IFN-α and -β were purchased from PBL Biomedical Laboratories. ELSA kit for mouse IL-6 was purchased from Invitrogen.

Preparation of Dendritic Cells and Macrophages

BM cells were prepared from the femur and tibia. The cells were cultured in RPMI1640 medium supplemented with 10% FCS, 100 μM 2-Me, and 100 ng/ml human Flt3 ligand (Pepro Tech), and 10 ng/ml murine GM-CSF or culture supernatant NIH 3T3 expressing M-CSF. After 6 days, cells were collected and used as Flt3L-DC, GM-DC, or BM-Mf. In the case of GM-DC or BM-Mf, the medium was changed every 2 days.

Native PAGE Analysis

Approximately 1 × 10^6 MEFs were infected with VSV at moi = 1 for 9 hr and then lysed. Cell lysates in native PAGE sample buffer (62.5 mM Tris-HCl [pH 6.8], 15% glycerol, and BPB) were separated using native PAGE and then immunoblotted with anti-murine IRF3 antibody (Zymed).

Luciferase Assay

Expression plasmids for mouse RIG-I N-terminal CARDs, full-length RIG-I, or full-length MDA5 were constructed in pEF-BOS. The cDNA fragment encoding the ORF of RIG-I or MDA5 was amplified by RT-PCR using total RNA prepared from MEFs. The Riplet dRING mutant protein lacks 1–69 aa region. Wild-type and mutant (Riplet dRING) Riplet-expression vectors were described previously (Oshiumi et al., 2009). Wild-type or *Riplet*$^{-/-}$ MEFs were transiently transfected in 24-well plates with reporter constructs containing the IFN-β promoter and Renilla luciferase (internal control) together with the empty vector (control), RIG-I CARDs, full-length RIG-I, or MDA5 expression vectors. Twenty-four hours after transfection, cells were lysed and subjected to the luciferase assay using the Dual-Luciferase Reporter Assay system (Promega).

Statistical Analyses

Statistical significance of differences between groups was determined by the Student's t test, and survival curves were analyzed by the log rank test using Prism 4 for Macintosh software (GraphPad Sofware, Inc.). Chi-square goodness-of-fit tests and Student's t tests were performed using MS-Excel software and a chi-square distribution table.

SUPPLEMENTAL INFORMATION

Supplemental Information includes five figures, one table, and Supplemental Experimental Procedures and can be found with this article at doi:10.1016/j.chom.2010.11.008.

ACKNOWLEDGMENTS

We thank Dr. John P. Atkinson (Washington University) and Dr. Ralph Steinman (Rockefeller University) for critical discussions, Yoko Esaki and Kiyo Kawata for technical support in generating Riplet KO mice, N. Irie for a pilot study of B-DNA stimulation assay, and Sakoda Y. for technical instructions for the experiments using Flu and SeV. This work was supported in part by the Mitsubishi Foundation; Mochida Foundation; Akiyama Life Science Foundation; and Grants-in-Aid from Ministry of Education, Science, and Culture and Ministry of Health, Labor, and Welfare of Japan.

Received: June 4, 2010
Revised: August 18, 2010
Accepted: November 5, 2010
Published: December 15, 2010

REFERENCES

Akira, S., Uematsu, S., and Takeuchi, O. (2006). Pathogen recognition and innate immunity. Cell *124*, 783–801.

Arimoto, K., Takahashi, H., Hishiki, T., Konishi, H., Fujita, T., and Shimotohno, K. (2007). Negative regulation of the RIG-I signaling by the ubiquitin ligase RNF125. Proc. Natl. Acad. Sci. USA *104*, 7500–7505.

Chiu, Y.H., Macmillan, J.B., and Chen, Z.J. (2009). RNA polymerase III detects cytosolic DNA and induces type I interferons through the RIG-I pathway. Cell *138*, 576–591.

Cui, S., Eisenacher, K., Kirchhofer, A., Brzozka, K., Lammens, A., Lammens, K., Fujita, T., Conzelmann, K.K., Krug, A., and Hopfner, K.P. (2008). The C-terminal regulatory domain is the RNA 5′-triphosphate sensor of RIG-I. Mol. Cell *29*, 169–179.

Diebold, S.S., Kaisho, T., Hemmi, H., Akira, S., and Reis e Sousa, C. (2004). Innate antiviral responses by means of TLR7-mediated recognition of single-stranded RNA. Science *303*, 1529–1531.

Douglas, J., Cilliers, D., Coleman, K., Tatton-Brown, K., Barker, K., Bernhard, B., Burn, J., Huson, S., Josifova, D., Lacombe, D., et al. (2007). Mutations in RNF135, a gene within the NF1 microdeletion region, cause phenotypic abnormalities including overgrowth. Nat. Genet. *39*, 963–965.

Gack, M.U., Shin, Y.C., Joo, C.H., Urano, T., Liang, C., Sun, L., Takeuchi, O., Akira, S., Chen, Z., Inoue, S., and Jung, J.U. (2007). TRIM25 RING-finger E3 ubiquitin ligase is essential for RIG-I-mediated antiviral activity. Nature *446*, 916–920.

Gack, M.U., Kirchhofer, A., Shin, Y.C., Inn, K.S., Liang, C., Cui, S., Myong, S., Ha, T., Hopfner, K.P., and Jung, J.U. (2008). Roles of RIG-I N-terminal tandem CARD and splice variant in TRIM25-mediated antiviral signal transduction. Proc. Natl. Acad. Sci. USA *105*, 16743–16748.

Gack, M.U., Albrecht, R.A., Urano, T., Inn, K.S., Huang, I.C., Carnero, E., Farzan, M., Inoue, S., Jung, J.U., and Garcia-Sastre, A. (2009). Influenza A virus NS1 targets the ubiquitin ligase TRIM25 to evade recognition by the host viral RNA sensor RIG-I. Cell Host Microbe *5*, 439–449.

Gao, D., Yang, Y.K., Wang, R.P., Zhou, X., Diao, F.C., Li, M.D., Zhai, Z.H., Jiang, Z.F., and Chen, D.Y. (2009). REUL is a novel E3 ubiquitin ligase and stimulator of retinoic-acid-inducible gene-I. PLoS ONE *4*, e5760. 10.1371/journal.pone.0005760.

Honda, K., Yanai, H., Takaoka, A., and Taniguchi, T. (2005). Regulation of the type I IFN induction: a current view. Int. Immunol. *17*, 1367–1378.

Honda, K., Takaoka, A., and Taniguchi, T. (2006). Type I interferon [corrected] gene induction by the interferon regulatory factor family of transcription factors. Immunity *25*, 349–360.

Horner, S.M., and Gale, M., Jr. (2009). Intracellular innate immune cascades and interferon defenses that control hepatitis C virus. J. Interferon Cytokine Res. *29*, 489–498.

Hornung, V., Ellegast, J., Kim, S., Brzozka, K., Jung, A., Kato, H., Poeck, H., Akira, S., Conzelmann, K.K., Schlee, M., et al. (2006). 5′-Triphosphate RNA is the ligand for RIG-I. Science *314*, 994–997.

Ishii, K.J., Coban, C., Kato, H., Takahashi, K., Torii, Y., Takeshita, F., Ludwig, H., Sutter, G., Suzuki, K., Hemmi, H., et al. (2006). A Toll-like receptor-independent antiviral response induced by double-stranded B-form DNA. Nat. Immunol. *7*, 40–48.

Ishii, K.J., Kawagoe, T., Koyama, S., Matsui, K., Kumar, H., Kawai, T., Uematsu, S., Takeuchi, O., Takeshita, F., Coban, C., and Akira, S. (2008). TANK-binding kinase-1 delineates innate and adaptive immune responses to DNA vaccines. Nature *451*, 725–729.

Ishikawa, H., and Barber, G.N. (2008). STING is an endoplasmic reticulum adaptor that facilitates innate immune signalling. Nature *455*, 674–678.

Ishikawa, H., Ma, Z., and Barber, G.N. (2009). STING regulates intracellular DNA-mediated, type I interferon-dependent innate immunity. Nature *461*, 788–792.

Kato, H., Sato, S., Yoneyama, M., Yamamoto, M., Uematsu, S., Matsui, K., Tsujimura, T., Takeda, K., Fujita, T., Takeuchi, O., and Akira, S. (2005). Cell type-specific involvement of RIG-I in antiviral response. Immunity *23*, 19–28.

Kato, H., Takeuchi, O., Sato, S., Yoneyama, M., Yamamoto, M., Matsui, K., Uematsu, S., Jung, A., Kawai, T., Ishii, K.J., et al. (2006). Differential roles of MDA5 and RIG-I helicases in the recognition of RNA viruses. Nature *441*, 101–105.

Kawai, T., Takahashi, K., Sato, S., Coban, C., Kumar, H., Kato, H., Ishii, K.J., Takeuchi, O., and Akira, S. (2005). IPS-1, an adaptor triggering RIG-I- and Mda5-mediated type I interferon induction. Nat. Immunol. *6*, 981–988.

Kumagai, Y., Takeuchi, O., Kato, H., Kumar, H., Matsui, K., Morii, E., Aozasa, K., Kawai, T., and Akira, S. (2007). Alveolar macrophages are the primary interferon-alpha producer in pulmonary infection with RNA viruses. Immunity *27*, 240–252.

Kumar, H., Kawai, T., Kato, H., Sato, S., Takahashi, K., Coban, C., Yamamoto, M., Uematsu, S., Ishii, K.J., Takeuchi, O., and Akira, S. (2006). Essential role of IPS-1 in innate immune responses against RNA viruses. J. Exp. Med. *203*, 1795–1803.

Meylan, E., Curran, J., Hofmann, K., Moradpour, D., Binder, M., Bartenschlager, R., and Tschopp, J. (2005). Cardif is an adaptor protein in the RIG-I antiviral pathway and is targeted by hepatitis C virus. Nature *437*, 1167–1172.

Miranda, C., Roccato, E., Raho, G., Pagliardini, S., Pierotti, M.A., and Greco, A. (2006). The TFG protein, involved in oncogenic rearrangements, interacts with TANK and NEMO, two proteins involved in the NF-kappaB pathway. J. Cell. Physiol. *208*, 154–160.

Nakhaei, P., Genin, P., Civas, A., and Hiscott, J. (2009). RIG-I-like receptors: sensing and responding to RNA virus infection. Semin. Immunol. *21*, 215–222.

Onoguchi, K., Yoneyama, M., Takemura, A., Akira, S., Taniguchi, T., Namiki, H., and Fujita, T. (2007). Viral infections activate types I and III interferon genes through a common mechanism. J. Biol. Chem. *282*, 7576–7581.

Oshiumi, H., Matsumoto, M., Hatakeyama, S., and Seya, T. (2009). Riplet/RNF135, a RING finger protein, ubiquitinates RIG-I to promote interferon-beta induction during the early phase of viral infection. J. Biol. Chem. *284*, 807–817.

Pichlmair, A., Schulz, O., Tan, C.P., Naslund, T.I., Liljestrom, P., Weber, F., and Reis e Sousa, C. (2006). RIG-I-mediated antiviral responses to single-stranded RNA bearing 5′-phosphates. Science *314*, 997–1001.

Rehwinkel, J., Tan, C.P., Goubau, D., Schulz, O., Pichlmair, A., Bier, K., Robb, N., Vreede, F., Barclay, W., Fodor, E., and Reis e Sousa, C. (2010). RIG-I detects viral genomic RNA during negative-strand RNA virus infection. Cell *140*, 397–408.

Saito, T., Hirai, R., Loo, Y.M., Owen, D., Johnson, C.L., Sinha, S.C., Akira, S., Fujita, T., and Gale, M., Jr. (2007). Regulation of innate antiviral defenses through a shared repressor domain in RIG-I and LGP2. Proc. Natl. Acad. Sci. USA *104*, 582–587.

Saito, T., Owen, D.M., Jiang, F., Marcotrigiano, J., and Gale, M., Jr. (2008). Innate immunity induced by composition-dependent RIG-I recognition of hepatitis C virus RNA. Nature *454*, 523–527.

Seth, R.B., Sun, L., Ea, C.K., and Chen, Z.J. (2005). Identification and characterization of MAVS, a mitochondrial antiviral signaling protein that activates NF-kappaB and IRF 3. Cell *122*, 669–682.

Shigemoto, T., Kageyama, M., Hirai, R., Zheng, J., Yoneyama, M., and Fujita, T. (2009). Identification of loss of function mutations in human genes encoding RIG-I and MDA5: implications for resistance to type I diabetes. J. Biol. Chem. *284*, 13348–13354.

Sun, Q., Sun, L., Liu, H.H., Chen, X., Seth, R.B., Forman, J., and Chen, Z.J. (2006). The specific and essential role of MAVS in antiviral innate immune responses. Immunity *24*, 633–642.

Suzuki, H., Fukunishi, Y., Kagawa, I., Saito, R., Oda, H., Endo, T., Kondo, S., Bono, H., Okazaki, Y., and Hayashizaki, Y. (2001). Protein-protein interaction panel using mouse full-length cDNAs. Genome Res. *11*, 1758–1765.

Takahasi, K., Yoneyama, M., Nishihori, T., Hirai, R., Kumeta, H., Narita, R., Gale, M., Jr., Inagaki, F., and Fujita, T. (2008). Nonself RNA-sensing mechanism of RIG-I helicase and activation of antiviral immune responses. Mol. Cell *29*, 428–440.

Takeuchi, O., and Akira, S. (2010). Pattern recognition receptors and inflammation. Cell *140*, 805–820.

Xu, L.G., Wang, Y.Y., Han, K.J., Li, L.Y., Zhai, Z., and Shu, H.B. (2005). VISA is an adapter protein required for virus-triggered IFN-beta signaling. Mol. Cell *19*, 727–740.

Yoneyama, M., and Fujita, T. (2009). RNA recognition and signal transduction by RIG-I-like receptors. Immunol. Rev. *227*, 54–65.

Yoneyama, M., and Fujita, T. (2010). Recognition of viral nucleic acids in innate immunity. Rev. Med. Virol. *20*, 4–22.

Yoneyama, M., Kikuchi, M., Natsukawa, T., Shinobu, N., Imaizumi, T., Miyagishi, M., Taira, K., Akira, S., and Fujita, T. (2004). The RNA helicase RIG-I has an essential function in double-stranded RNA-induced innate antiviral responses. Nat. Immunol. *5*, 730–737.

Zeng, W., Sun, L., Jiang, X., Chen, X., Hou, F., Adhikari, A., Xu, M., and Chen, Z.J. (2010). Reconstitution of the RIG-I pathway reveals a signaling role of unanchored polyubiquitin chains in innate immunity. Cell *141*, 315–330.

Immunity
Article

Cell-Cell Propagation of NF-κB Transcription Factor and MAP Kinase Activation Amplifies Innate Immunity against Bacterial Infection

Christoph Alexander Kasper,[1] Isabel Sorg,[1] Christoph Schmutz,[1] Therese Tschon,[1] Harry Wischnewski,[1] Man Lyang Kim,[1] and Cécile Arrieumerlou[1,*]
[1]Biozentrum, University of Basel, Klingelbergstrasse 50-70, CH-4056, Basel, Switzerland
*Correspondence: cecile.arrieumerlou@unibas.ch
DOI 10.1016/j.immuni.2010.10.015

SUMMARY

The enteroinvasive bacterium *Shigella flexneri* uses multiple secreted effector proteins to downregulate interleukin-8 (IL-8) expression in infected epithelial cells. Yet, massive IL-8 secretion is observed in Shigellosis. Here we report a host mechanism of cell-cell communication that circumvents the effector proteins and strongly amplifies IL-8 expression during bacterial infection. By monitoring proinflammatory signals at the single-cell level, we found that the activation of the transcription factor NF-κB and the MAP kinases JNK, ERK, and p38 rapidly propagated from infected to uninfected adjacent cells, leading to IL-8 production by uninfected bystander cells. Bystander IL-8 production was also observed during *Listeria monocytogenes* and *Salmonella typhimurium* infection. This response could be triggered by recognition of peptidoglycan and is mediated by gap junctions. Thus, we have identified a mechanism of cell-cell communication that amplifies innate immunity against bacterial infection by rapidly spreading proinflammatory signals via gap junctions to yet uninfected cells.

INTRODUCTION

The ability of a host organism to mount an innate immune response after pathogen infection is critical for survival. The epithelial cells, which represent the first physical barrier to invasive pathogens, play a critical role in this process. They act as sentinels of the immune system and largely contribute to the secretion of factors that orchestrate inflammation in infected tissues. Infection by *Shigella* bacteria is a well-suited model to analyze the complex host-pathogen interactions that shape the immune response of intestinal epithelial cells (IECs) to invasive bacteria (Phalipon and Sansonetti, 2007). *Shigella* are Gram-negative foodborne bacteria that invade the colonic and rectal epithelium of humans, causing an acute mucosal inflammation called Shigellosis, responsible for 1.1 million deaths annually (Schroeder and Hilbi, 2008).

Shigella flexneri, the etiological agent of the most endemic form of Shigellosis, translocates across the intestinal epithelial barrier by transcytosis through M cells. In the submucosal area, *S. flexneri* makes use of a type III secretion (T3S) apparatus to trigger apoptosis in macrophages and to actively invade IECs via their basolateral surface. The T3S apparatus is a syringe-like nanomachine enabling the translocation of bacterial effector proteins (Cornelis, 2006) that subvert various host cellular pathways in order to promote bacterial entry, modulate cell cycle, and dampen inflammation signaling (Iwai et al., 2007; Parsot, 2009; Phalipon and Sansonetti, 2007). Once internalized, *S. flexneri* multiplies in the cytoplasm and uses actin-based motility to spread to adjacent IECs. During infection, massive mucosal inflammation is observed in the intestine of infected patients (Islam et al., 1997). IECs are critical in this process. They sense pathogenic invasion and respond by inducing a transcriptional program whose major function is to stimulate innate immune defense mechanisms. *Shigella* recognition by IECs occurs essentially intracellularly via the pattern recognition receptor Nod1 that recognizes the core dipeptide structure, γ-D-glutamyl-meso-diaminopimelic acid (Girardin et al., 2003), found in the peptidoglycan of all Gram-negative and certain Gram-positive bacteria (Kufer et al., 2006). Upon ligand recognition, Nod1 homodimerizes and recruits the kinase RIPK2 (Strober et al., 2006). This leads to the sequential recruitment and activation of the TAK1-TAB1-TAB2 and IKKα-IKKβ-IKKγ complexes and the phosphorylation of inhibitor of NF-κB alpha (IκBα). Once phosphorylated, IκBα undergoes polyubiquitination and proteasomal degradation. NF-κB, released from IκBα, translocates to the nucleus and upregulates expression of proinflammatory genes. TAK1 activation also leads to activation of the MAP kinases c-Jun-N-terminal kinase (JNK) and p38 (Lee et al., 2000; Ninomiya-Tsuji et al., 1999; Wang et al., 2001). The MAP kinase ERK is also activated during *S. flexneri* infection of IECs (Köhler et al., 2002). NF-κB, JNK, ERK, and p38 contribute collectively to the initiation of a proinflammatory program. JNK and p38 regulate the activity of the transcription factor AP-1 (Holtmann et al., 1999). p38 and ERK control the access of chromatin to transcription factors via phosphorylation of histone H3 by the kinases MSK1 and MSK2 (Saccani et al., 2002). Among the genes upregulated during infection of IECs, the chemokine interleukin-8 (IL-8) plays a central role (Sansonetti et al., 1999) by attracting polymorphonuclear cells (PMNs) from the peripheral circulation to the infected area to limit the spread of *S. flexneri* invasion.

S. flexneri uses multiple strategies to downregulate inflammation. For example, T3 secreted effector proteins OspG and OspF attenuate IL-8 expression by preventing IκBα degradation and dephosphorylating nuclear p38 and ERK, respectively (Arbibe et al., 2007; Kim et al., 2005; Li et al., 2007).

Despite the immunosuppressive activity of multiple bacterial effector proteins, massive IL-8 expression is observed in IECs during Shigellosis, suggesting that the secreted molecules may partially block IL-8 expression or that a host mechanism compensates for their effect. Here, we report the discovery of a host cell-cell communication mechanism that circumvents the bacterial effector proteins and amplifies IL-8 expression. By monitoring proinflammatory signals at the single-cell level, we found that, within minutes of infection, the activation of NF-κB and the MAP kinases JNK, ERK, and p38, propagates from infected to uninfected bystander cells. These cells, in which signaling is not altered by bacterial effector proteins, represent the main source of IL-8 secretion during *S. flexneri* infection. Bystander IL-8 expression can be triggered by recognition of peptidoglycan via Nod1 and is mediated by gap junctions. Thus, we have identified a gap junction-mediated cell-cell communication mechanism that strongly amplifies innate immunity during bacterial infection by rapidly spreading proinflammatory signals to yet-uninfected cells.

RESULTS

NF-κB Is Activated in Bystander Cells of *S. flexneri* Infection

To better characterize the molecular mechanisms that control inflammation during bacterial infection, we analyzed NF-κB activation at the single-cell level during *S. flexneri* infection of epithelial cells. The nuclear translocation of the NF-κB p65 subunit, which follows IKK-mediated IκBα degradation, was used as readout for NF-κB activation and was visualized by immunofluorescence microscopy. HeLa cells were infected with noninvasive BS176 or wild-type invasive M90T *S. flexneri* strains at low and high multiplicity of infection (MOI). As expected, extracellular bacteria failed to activate NF-κB in HeLa cells as shown by the fact that p65 remained exclusively cytosolic after infection with BS176 *S. flexneri* (Figure 1A, top left). In contrast, cells infected with M90T at MOI 20 showed massive nuclear localization of p65, reflecting the detection of intracellular bacteria and activation of NF-κB (Figure 1A, top right). Surprisingly, when cells were challenged with M90T at low MOI, a strong p65 nuclear translocation was also observed in some cells that were not infected (Figure 1A, bottom left). Single-cell measurements of *S. flexneri* invasion and p65 nuclear/cytoplasmic ratio (NF-κB activation ratio) confirmed that, at low MOI, more cells were NF-κB activated than infected (Figure 1A, bottom right). False color representations of the NF-κB activation ratio clearly showed that uninfected NF-κB-activated cells were not randomly distributed in the field of view but located in close proximity with infected cells forming NF-κB activation foci around them (Figure 1B). A similar pattern of NF-κB activation was observed during *S. flexneri* infection of the colonic epithelial cell line Caco-2, the lung epithelial cell line A549, and the human umbilical vein endothelial cells (HUVECs) derived from umbilical cord (Figure S1 available online), suggesting that bystander activation of NF-κB represents a broad response to *S. flexneri* infection.

During infection, *S. flexneri* uses actin-based motility to spread to adjacent IECs. To control that bystander NF-κB activation was not due to bacterial intercellular motility, we examined NF-κB activation in cells infected with the nonmotile *virG* deletion mutant (Δ*virG*) (Makino et al., 1986). As expected, Δ*virG* bacteria efficiently invaded HeLa cells (Figure 1C, right). However, unlike wild-type (Figure 1C, left), they failed to form actin comet tails and accumulated overtime in the perinuclear region (Figure 1C, right). Interestingly, infection with the Δ*virG* mutant induced p65 nuclear translocation in infected and in bystander cells (Figure 1D) similarly to infection with wild-type *S. flexneri* (Figure 1A), suggesting that bystander NF-κB activation was not caused by intercellular motility, but reflected instead a novel host response to bacterial infection. Because the intracellular microcolonies formed by the Δ*virG* mutant were easily detected by automated image analysis, this mutant was used hereafter in our studies.

In order to further characterize bystander NF-κB activation, we analyzed its kinetic during *S. flexneri* infection in HeLa cells. Representative examples of bystander activation at different time points were chosen for illustration (Figure 1E). Within 15 min of infection, NF-κB was almost exclusively activated in infected cells. Then, at 30 min and up to 120 min, NF-κB activation was observed in infected and bystander cells, suggesting that the signals underlying bystander NF-κB activation were generated very early during infection (within 30 min) and propagated from infected to bystander cells. Considering that each infected cell was surrounded by approximately 2–6 NF-κB-activated cells, our results demonstrate that this mechanism of cell-cell communication strongly amplifies the total NF-κB response to *S. flexneri* infection.

JNK and ERK Are Also Activated in Bystander Cells of *S. flexneri* Infection

The activation of the JNK signaling pathway is required to mount an inflammatory response, and in particular, to induce IL-8 expression. We therefore tested, whether in addition to NF-κB, the JNK pathway was also activated in bystander cells of *S. flexneri* infection in HeLa and Caco-2 cells. JNK activation was analyzed by immunofluorescence microscopy via a phospho-specific antibody that detects p46 and p54 JNKs phosphorylated at residues threonine 183 and tyrosine 185 (p-JNK). Cytosolic p65 localization and basal p-JNK staining indicated that both pathways were inactive in control cells (Figure 2A). As expected, a clear nuclear translocation of p65 and a significant increase of p-JNK were observed in *S. flexneri*-infected cells. Interestingly, bystander cells of infection also showed an increase of p-JNK, indicating that the JNK pathway was turned on in these cells as well (Figure 2A and Figure S2A). This observation was confirmed by measuring with automated image processing the degree of nuclear p-JNK in control, infected, and bystander cell populations (Figure 2B, see Supplemental Experimental Procedures).

In addition to JNK, the activation of ERK was analyzed by immunofluorescence microscopy by means of an antibody that recognizes p22 and p44 ERKs phosphorylated at residues threonine 202 and tyrosine 204 (p-ERK). Representative images of NF-κB and p-ERK at different time points were chosen for

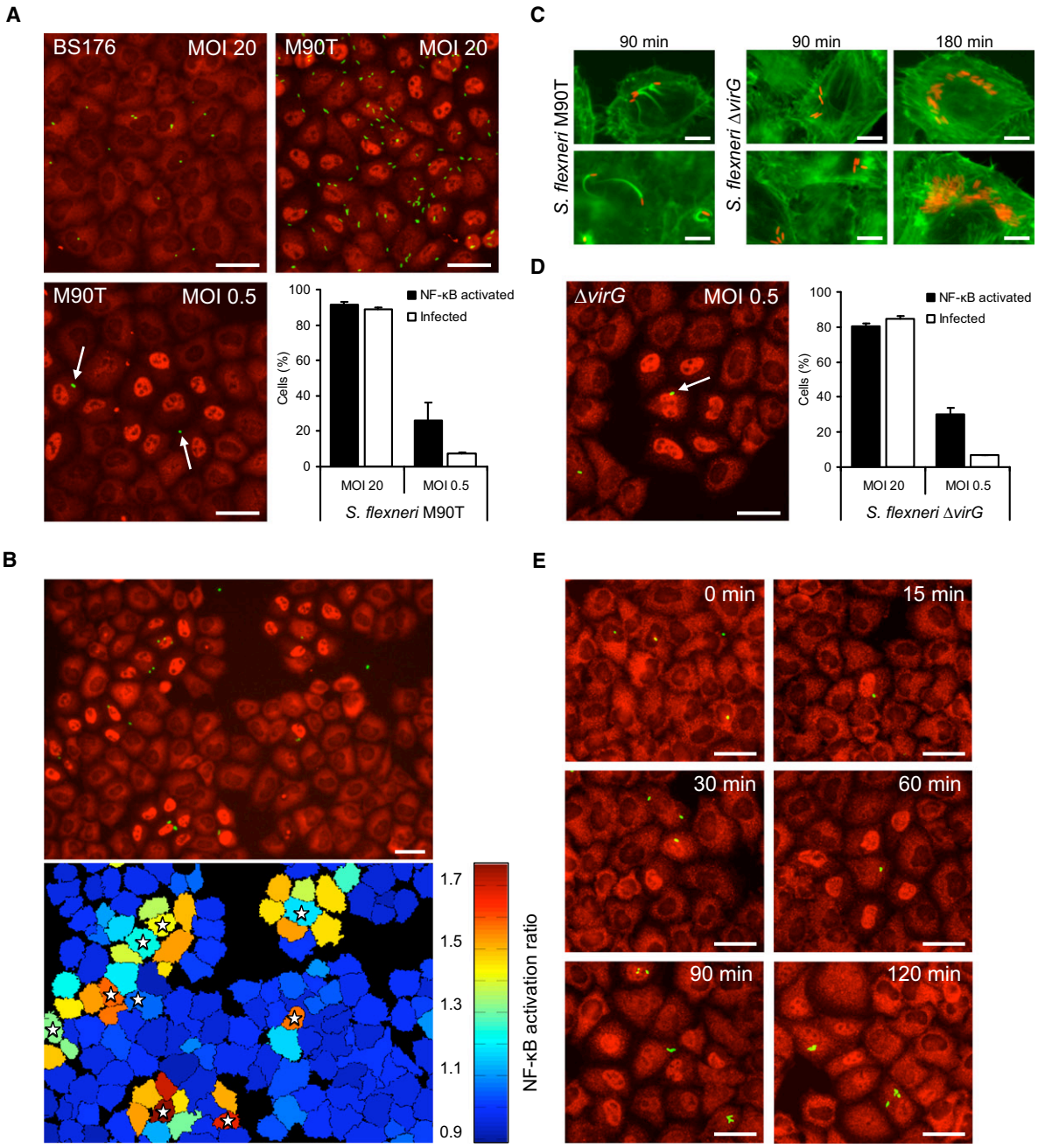

Figure 1. NF-κB Is Activated in Bystander Cells of *S. flexneri* Infection

(A) Nuclear localization of NF-κB p65 during *S. flexneri* infection. HeLa cells were infected for 1 hr with BS176 (MOI = 20, top left) and M90T (MOI = 20, top right; MOI = 0.5, bottom left), stained with a p65 antibody, and visualized by fluorescence microscopy (p65 in red, *S. flexneri* in green). Arrows indicate *S. flexneri*. Percent of NF-κB activated and infected cells at high and low MOI (bottom right, means ± SD of triplicate wells, graph representative of two independent experiments). Scale bars represent 40 μm.

(B) False color representation of NF-κB activation ratio during *S. flexneri* M90T infection of HeLa cells. Stars indicate infected cells. Scale bar represents 40 μm.

(C) Actin-based motility of *S. flexneri* M90T (left) and Δ*virG* mutant (right). After infection, cells were stained for F-actin with phalloidin (F-actin in green, *S. flexneri* in red). Scale bars represent 10 μm.

(D) Bystander NF-κB activation during infection with *S. flexneri* Δ*virG* (left). p65 in red, *S. flexneri* in green. Arrow indicates *S. flexneri*. Percent of NF-κB activated and infected cells at high and low MOI (right, means ± SD of triplicate wells, graph representative of two independent experiments). Scale bar represents 40 μm.

(E) Time course of p65 translocation during infection with *S. flexneri* Δ*virG*. Representative images were selected for illustration. Scale bars represent 40 μm.

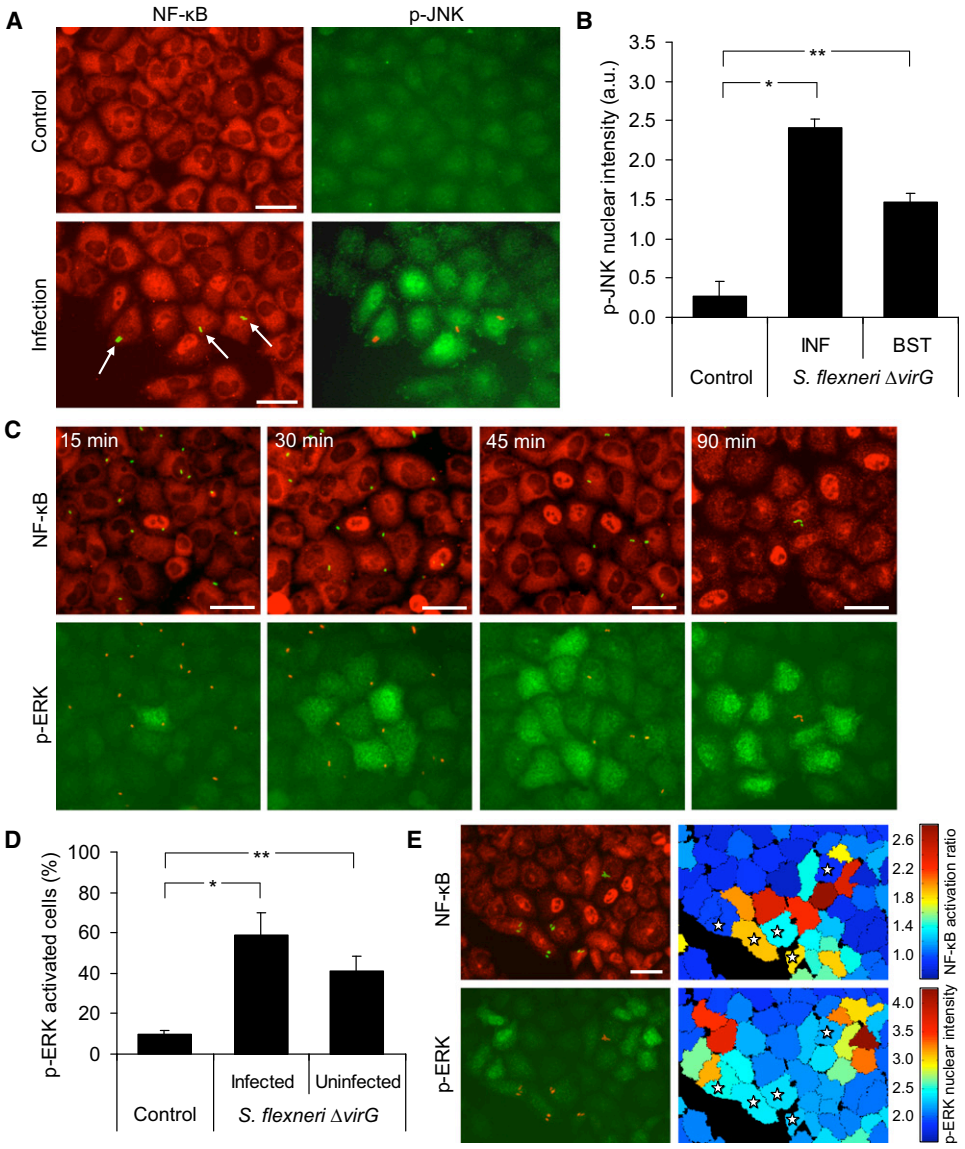

Figure 2. JNK and ERK Are Activated in Bystander Cells of *S. flexneri* Infection

(A) Analysis of JNK and NF-κB activation by immunofluorescence microscopy. HeLa cells were left untreated or infected with *S. flexneri* Δ*virG* at MOI = 0.5 for 90 min and costained with p65 and p-JNK antibodies. Arrows indicate *S. flexneri*. Scale bars represent 40 μm.

(B) Quantification of nuclear p-JNK intensity in control, infected (INF), and bystander (BST) cell populations by automated image processing (a.u., arbitrary units, means ± SD of triplicate wells, graph representative of five independent experiments, *p = 7.2E-5, **p = 7.6E-4).

(C) Time course of ERK and NF-κB activation during infection with *S. flexneri.* HeLa cells were infected with *S. flexneri* Δ*virG* at MOI = 0.5 for indicated time periods and costained with p65 and p-ERK antibodies. Scale bars represent 40 μm.

(D) Percent of ERK-activated cells during *S. flexneri* infection. Cells were infected for 1 hr at MOI = 5. Quantification was performed by automated image processing as described in Supplemental Experimental Procedures (means ± SD of triplicate wells, graph representative of three independent experiments, *p = 1.9E-3, **p = 4.7E-3).

(E) False color representations of NF-κB activation ratio and nuclear p-ERK 1 hr after infection with *S. flexneri* Δ*virG*. Stars indicate infected cells. Scale bar represents 40 μm.

illustration (Figure 2C). Within 15 min of infection, ERK activation was observed in only a fraction of infected cells. At 30 min and up to 90 min, ERK was also activated in bystander cells of infection (Figures 2C and 2D and Figure S2B). NF-κB and ERK activation did not strictly correlate at the single-cell level. Indeed, after 45 min of infection, ERK activation was no longer visible in a fraction of infected or proximal bystander cells, suggesting that this pathway was only transiently induced. Furthermore, ERK activation was observed in cells located outside the NF-κB activation foci, suggesting that ERK activation preceded NF-κB activation (Figures 2C and 2E). Altogether, these results suggested that besides the activation of NF-κB, the activation of JNK and ERK also propagates from infected to bystander cells during *S. flexneri* infection of HeLa and Caco-2 cells.

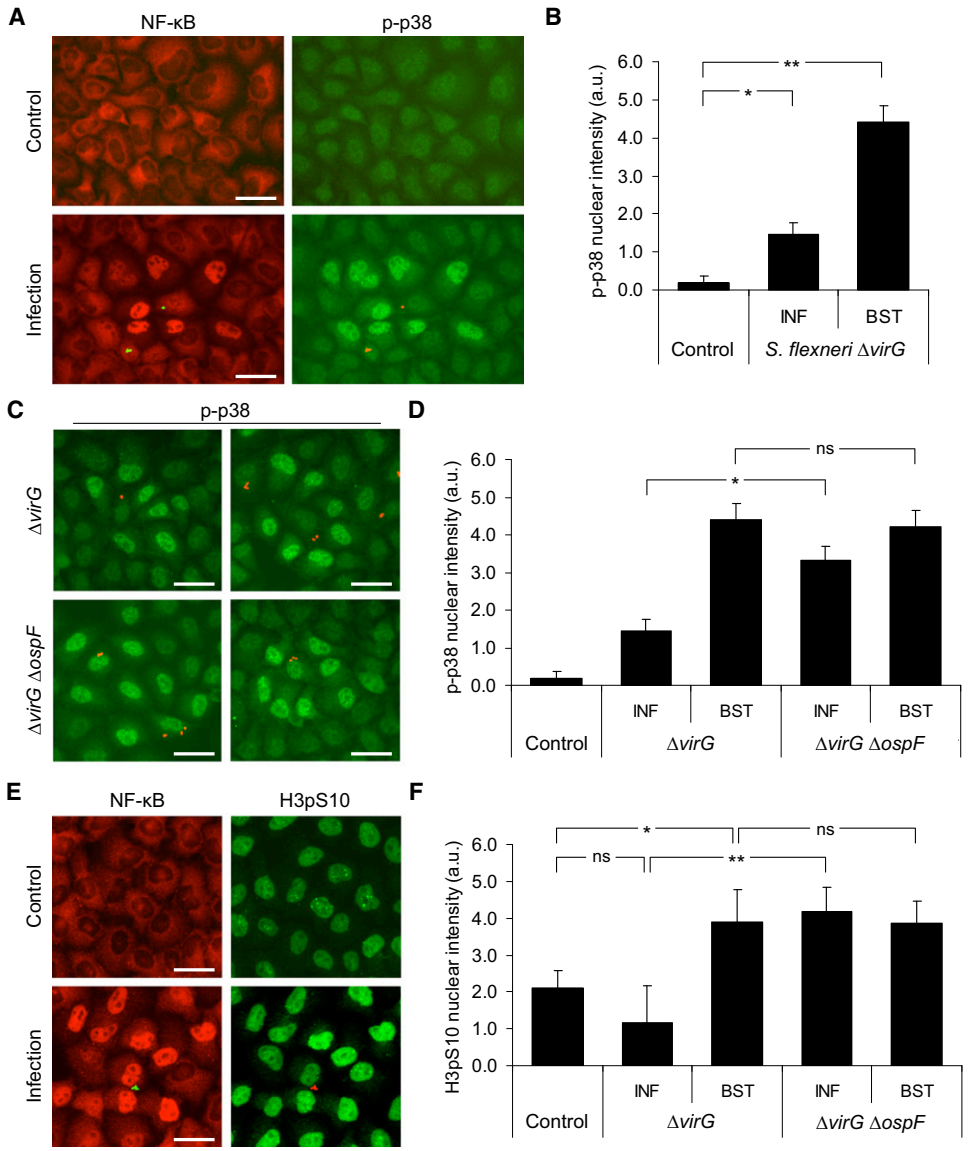

Figure 3. p38 Activation and Histone H3 Phosphorylation Occur Mainly in Bystander Cells

(A) Analysis of p38 and NF-κB activation by immunofluorescence microscopy. HeLa cells were left untreated or infected with *S. flexneri* Δ*virG* at MOI = 0.5 for 90 min and costained with p65 and p-p38 antibodies. Scale bars represent 40 μm.

(B) Quantification of nuclear p-p38 intensity in control, infected (INF), and bystander (BST) cell populations (a.u., arbitrary units, means ± SD of triplicate wells, graph representative of five independent experiments, *p = 4.1E-3, **p = 1.0E-4).

(C) Phosphorylation of p38 in cells infected with Δ*virG* or Δ*virG* Δ*ospF S. flexneri* visualized by immunofluorescence microscopy. Scale bars represent 40 μm.

(D) Quantification of nuclear p-p38 intensity by automated image processing in control, infected, and bystander cell populations during infection with Δ*virG* or Δ*virG* Δ*ospF S. flexneri* (means ± SD of triplicate wells, graph representative of five independent experiments, *p = 4.2E-3).

(E) Analysis of histone H3 phosphorylation by immunofluorescence microscopy. HeLa cells were left untreated or infected with *S. flexneri* Δ*virG* at MOI = 0.5 for 90 min and costained with p65 and H3pS10 antibodies. Scale bars represent 40 μm.

(F) Quantification of nuclear H3pS10 intensity in control, infected, and bystander cell populations (means ± SD of triplicate wells, graph representative of five independent experiments, *p = 4.9E-2, **p = 1.1E-3).

p38 Activation and Histone H3 Phosphorylation Mainly Occur in Bystander Cells of Infection

Because p38 activation is also critical for IL-8 expression, we examined whether p38 was activated in bystander cells of *S. flexneri* infection in HeLa and Caco-2 cells. p38 activation was analyzed by immunofluorescence microscopy by means of an antibody that detects p38 phosphorylated at residues threonine 180 and tyrosine 182 (p-p38). As reported previously (Arbibe et al., 2007), a very modest increase of p38 activation was observed in infected cells (Figures 3A and 3B and Figure S3). In contrast, a strong increase was found in bystander cells of infection indicating that, in addition to NF-κB, JNK, and ERK, p38 was also activated in these cells (Figures 3A and 3B and Figure S3). Signal transduction in infected cells is altered by multiple

effectors that translocate into the host cytoplasm via the T3S apparatus. In particular, p38 is dephosphorylated in the nucleus of infected cells by the phosphothreonine-lyase activity of OspF (Li et al., 2007). Given that bystander cells showed massive p38 activation, we hypothesized that the activation of p38 in bystander cells was not affected by OspF. To test this assumption, HeLa cells were infected with Δ*virG* and Δ*virG* Δ*ospF S. flexneri* mutants. As previously reported (Arbibe et al., 2007), p38 activation was restored in cells infected with Δ*ospF* bacteria, confirming the role of OspF in p38 dephosphorylation (Figures 3C and 3D). In contrast, the amount of p38 activation in bystander cells remained unchanged (Figure 3D), indicating that OspF failed to impair the ability of the host to spread p38 activation to neighboring cells. Taken together, our data showed that the mechanism of bystander p38 activation circumvents the suppressive activity of OspF in infected cells and amplifies p38 activation during *S. flexneri* infection.

In addition to its role in AP-1 phosphorylation, p38 controls IL-8 expression by regulating chromatin accessibility to transcription factors such as NF-κB via the phosphorylation of histone H3 by MSK1 and MSK2 (Saccani et al., 2002). To assess whether bystander p38 activation led to histone H3 phosphorylation in bystander cells, phosphorylation at serine 10 (H3pS10) was analyzed by immunofluorescence microscopy via a phospho-specific antibody. To minimize H3pS10 staining from mitotic cells, HeLa cells were arrested in S phase by a double-thymidine block. Consistent with the pattern of p38 activation during *S. flexneri* infection, H3pS10 was higher in bystander than infected cells (Figures 3E and 3F). Furthermore, the deletion of *ospF* restored H3pS10 in infected cells but had no effect in bystander cells (Figure 3F). Collectively, these results demonstrate that p38 activation and the subsequent phosphorylation of histone H3, which are both impaired in infected cells because of the activity of OspF, are fully operating in bystander cells of *S. flexneri* infection.

Cell-Cell Propagation of Proinflammatory Signals Amplifies Cytokine Expression

The NF-κB, JNK, ERK, and p38 signaling pathways were turned on in bystander cells of *S. flexneri* infection. Given that these pathways control the expression of proinflammatory genes including IL-8, we tested whether bystander cells of *S. flexneri* infection secreted IL-8. IL-8 secretion was first measured by an enzyme-linked immunosorbent assay (ELISA) in the supernatant of HeLa cells infected by *S. flexneri* at different MOIs. We observed that the amount of secreted IL-8 decreased as the MOI was raised (Figure 4A). Because low and high MOIs corresponded to low and high infected to bystander cell ratios, respectively (Figure S4A), this result suggested that IL-8 was most probably secreted by bystander cells of infection. This hypothesis was tested by in situ mRNA hybridization to visualize at the single-cell level the amount of IL-8 mRNA produced during *S. flexneri* infection. As shown in Figure 4B, IL-8 mRNAs were almost exclusively present in bystander cells of infection. To confirm that bystander cells were the main IL-8-producing cells during *S. flexneri* infection, we performed an intracellular IL-8 immunofluorescence microscopy assay in cells treated with monensin, a protein transport inhibitor that blocks secretion and enables intracellular IL-8 accumulation in the Golgi apparatus (Mollenhauer et al., 1990). In line with the ELISA and the mRNA data, almost no IL-8 was visible in infected cells, but massive intracellular IL-8 accumulation was found in bystander cells (Figures 4C and 4D). An average of 2.8 ± 1.6, 4.2 ± 2.5, 6.5 ± 4.7, and 29.3 ± 13.5 bystander IL-8-producing cells per infected one was measured in HeLa, Caco-2, A549, and HUVEC cells, respectively (Figures S4B–S4D). Interestingly, tumor necrosis factor α (TNF-α) and granulocyte macrophage colony-stimulating factor (GM-CSF), two other inflammatory cytokines upregulated during *S. flexneri* infection of epithelial cells (Pédron et al., 2003), were also found in bystander cells (Figures S4E–S4G), suggesting that the mechanism of bystander activation contributes to different facets of inflammation during infection.

Strong cytokine expression in bystander cells indicated that cell-cell communication was not affected by *S. flexneri* effector proteins. This was tested by investigating the effect of OspF on IL-8 expression in infected and bystander cell populations. As previously reported (Arbibe et al., 2007), an increase of IL-8 production was observed in cells infected with Δ*ospF S. flexneri* (Figure 4E). In contrast, the number of bystander cells producing IL-8 was independent of OspF (Figure 4F) indicating that, in line with our p38 activation and H3pS10 results, OspF failed to affect IL-8 expression in bystander cells.

To further characterize the mechanism of bystander activation, we tested whether it also occurred after infection with *Listeria monocytogenes* or *Salmonella typhimurium*, two enteroinvasive bacteria that induce IL-8 expression during invasion of IECs (Eckmann et al., 1993). Consistent with data on *S. flexneri* infection, IL-8 accumulation was also observed in bystander cells of *L. monocytogenes* and *S. typhimurium* infection (Figure 4G) but at a lower frequency. In conditions where bystander IL-8 expression was observed for nearly 100% of *S. flexneri*-infected cells, it occurred for approximately 40% and 70% of *Listeria*- and *Salmonella*-infected cells, respectively. In contrast to *S. flexneri* infection, IL-8 accumulation was also detected in a fraction of cells infected with *L. monocytogenes* or *S. typhimurium* (approximately 20% and 40%, respectively), indicating that these bacteria do not manipulate their host to the same extent as *S. flexneri,* for which low levels of IL-8 were detected in less than 5% of infected cells (Figure 4E). Altogether these results show that cell-cell communication between infected and uninfected bystander cells leads to the potentiation of inflammatory cytokine expression during bacterial infection. They also establish that this is a general host response to invasive bacteria that occurs with an amplitude and a frequency that vary between cell types and pathogens.

Nod1-Mediated Peptidoglycan Sensing Is Sufficient to Induce Bystander IL-8 Expression

During *S. flexneri* infection, the presence of intracellular bacteria is sensed through peptidoglycan recognition by the intracellular receptor Nod1 (Girardin et al., 2003). To determine whether pathogen sensing via Nod1 was sufficient to induce bystander IL-8 production, we monitored IL-8 accumulation after microinjection of the synthetic Nod1 ligand L-Ala-D-γ-Glu-meso-diaminopimelic acid (TriDAP) into the cytoplasm of A549 cells. An Alexa 488-labeled IgG antibody (IgG A488) was used as fluorescent marker to identify microinjected cells. In response to IgG A488 microinjection, no IL-8 was detected (Figure 5A, left, and

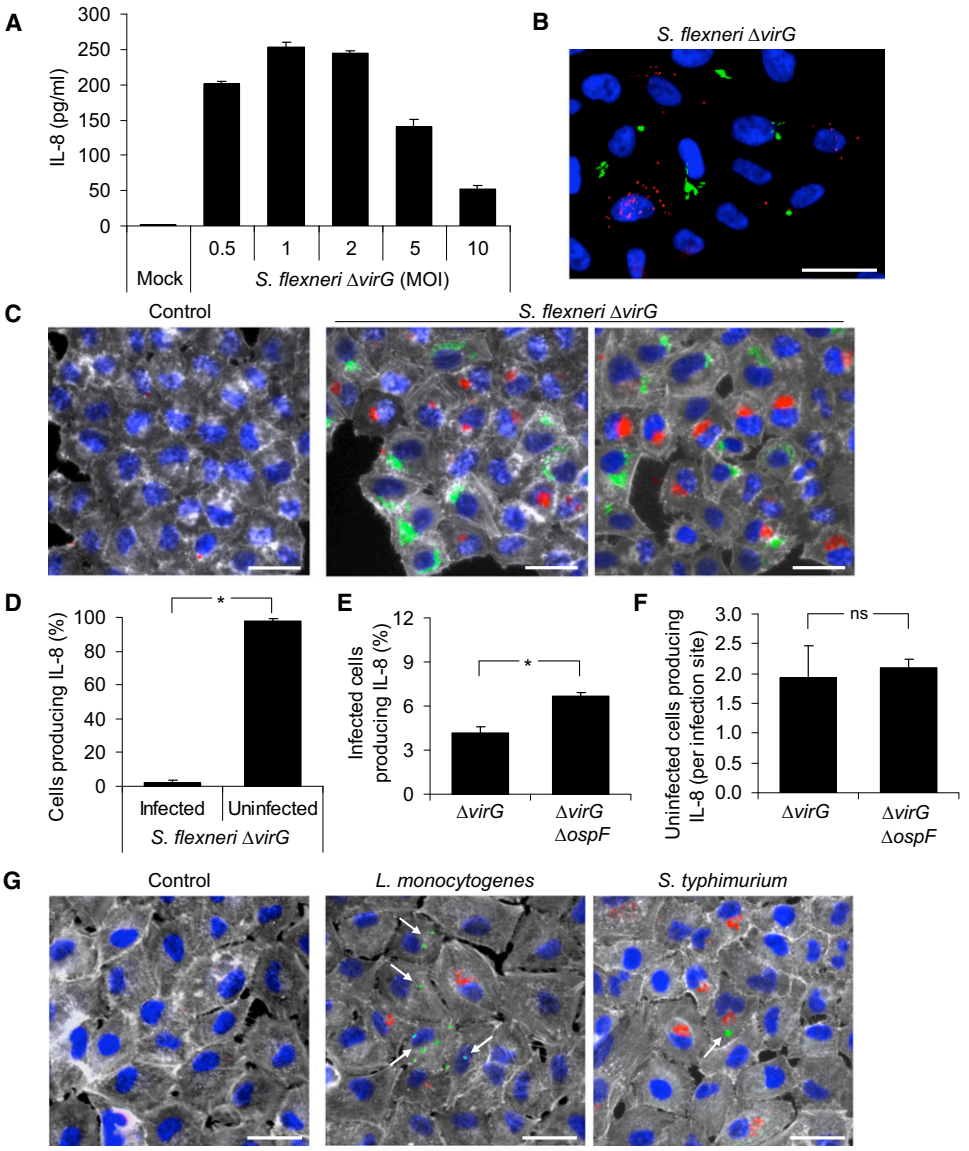

Figure 4. IL-8 Production by Bystander Cells Is a General Response to Bacterial Infection

(A) Measurements of IL-8 secretion by ELISA 6 hr after infection (means ± SD of triplicate wells, graph representative of two independent experiments).

(B) Visualization of IL-8 mRNA 2 hr after infection by in situ hybridization (IL-8 mRNAs in red, *S. flexneri* in green, Hoechst in blue, MOI = 2). Scale bar represents 40 μm.

(C) IL-8 accumulation in bystander cells of infection. IL-8 staining of monensin-treated HeLa cells 3 hr after infection (IL-8 in red, *S. flexneri* in green, Hoechst in blue, F-actin in gray, MOI = 2). Scale bars represent 40 μm.

(D) Percent of infected and uninfected cells among all IL-8-producing cells (MOI = 1). Quantification was performed by automated image processing based on the use of threshold intensity values for bacterial and IL-8 detection (means ± SD of triplicate wells, graph representative of three independent experiments, *p = 3.9E-16).

(E) Percent of infected cells producing IL-8 during infection with Δ*virG* and Δ*virG* Δ*ospF S. flexneri* (MOI = 5). Quantification was performed as described in (D) (means ± SD of triplicate wells, graph representative of two independent experiments, *p = 4.5E-4).

(F) Number of uninfected cells producing IL-8 per site of infection during infection with Δ*virG* and Δ*virG* Δ*ospF S. flexneri* (MOI = 1). Quantification was performed as described in (D) (means ± SD of triplicate wells, graph representative of two independent experiments).

(G) IL-8 production (in red) in bystander cells during *L. monocytogenes* (MOI = 0.25, green) and *S. typhimurium* (MOI = 0.5, green) infection of A549 cells. F-actin in gray, arrows indicate bacteria. Scale bars represent 40 μm.

Figure 5B). In contrast, when TriDAP was combined with IgG A488, both microinjected and bystander cells showed massive intracellular IL-8 accumulation (Figure 5A, right, and Figure 5B). To verify that IL-8 production was not caused by extracellular TriDAP leaking during microinjection, the concentration of TriDAP used in the microcapillary was uniformly applied to the extracellular medium. In contrast to TNF-α, extracellular TriDAP failed to induce IL-8 expression (Figure 5C and Figure S5).

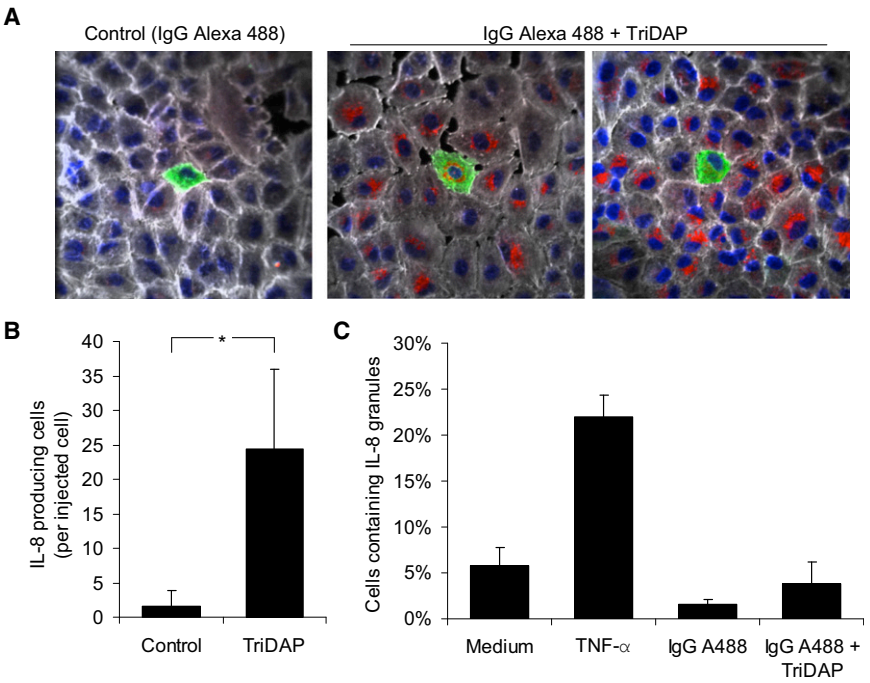

Figure 5. Intracellular Recognition of a Nod1 Ligand Is Sufficient to Induce IL-8 Expression in Bystander Cells

(A) IL-8 accumulation in bystanders of microinjected A549 cells. After injection of IgG Alexa 488 alone (left) or combined with TriDAP (right), cells were stained for IL-8, F-actin, and DNA (IgG A488 in green, IL-8 in red, F-actin in gray, Hoechst in blue).

(B) Number of IL-8-producing cells per injected cell. Quantification was performed by counting all IL-8-expressing cells located in contact with microinjected cells or other bystander cells (control, n = 20; TriDAP, n = 21; *p = 1.0E-9).

(C) Percent of cells containing IL-8 after extracellular treatment with TNF-α, IgG A488 alone, or combined with TriDAP. Cells were stained for IL-8 and DNA and analyzed by automated image processing (means ± SD of triplicate wells, graph representative of two independent experiments).

Together, these results suggested that Nod1-mediated recognition of intracellular TriDAP was necessary and sufficient to induce IL-8 expression by bystander cells of microinjection. Because Nod1-mediated recognition of peptidoglycan also takes place in *S. flexneri*-infected cells, this result suggested that pathogen sensing may be sufficient to trigger IL-8 expression in bystander cells of *S. flexneri* infection.

Bystander Activation Is Not Mediated by Paracrine Signaling but Requires Cell-Cell Contact

Reports indicating that TNF-α is upregulated during *S. flexneri* infection and that NF-κB, p38, ERK, and JNK are activated by TNF-α suggested that this cytokine may induce bystander activation via paracrine signaling (Dong et al., 2002; Pédron et al., 2003). This hypothesis was tested by examining bystander activation in tumor necrosis factor receptor 1 (TNFR1)-deficient mouse embryonic fibroblasts (*Tnfr1*$^{-/-}$ MEFs). Because mice are deficient for the *IL8* gene, the chemokine macrophage inflammatory protein-2 (MIP-2) was chosen as readout of inflammation. Whereas *Tnfr1*$^{-/-}$ cells did not respond to TNF-α stimulation, massive MIP-2 expression was observed in bystander cells of *S. flexneri* infection (Figure 6A; Figures S6A and S6B), indicating that TNF-α was not the mediator of bystander activation. To investigate the role of protein secretion more broadly, we tested whether this process was impaired when protein secretion was abolished by the protein transport inhibitor brefeldin A (BFA). For conditions of drug treatment that blocked phorbol 12-myristate 13-acetate (PMA)-induced IL-8 secretion (Figure S6C), BFA had no effect on bystander activation during *S. flexneri* infection of Caco-2 cells (Figures 6B and 6C), suggesting that cell-cell propagation of proinflammatory signals was not mediated by secreted proteins.

To further explore the hypothesis of paracrine signaling, experiments of *S. flexneri* infection were performed in a flow chamber where fresh medium was perfused to wash away any potential secreted factors. A flow rate corresponding to the replacement of the entire volume of the chamber every second was used. IL-8 accumulation was still visible in bystander cells of infection located along an axis perpendicular or opposite to the direction of the flow (Figure S6D). Quantification of IL-8 (Figure 6D) showed no effect of perfusion, indicating that bystander activation was very improbably mediated by a long-ranged diffusing soluble factor.

To characterize the mechanism of bystander activation, we investigated whether it was cell-cell contact dependent. Infection was performed at subconfluent cell density to evaluate IL-8 expression in Caco-2 cells that had no physical interactions with infected cells. Inspection of images and manual quantification indicated that IL-8 was exclusively found in cells having direct or indirect contacts with infected cells and defined as class 1 (Figures 6E and 6F). Class 2 cells present in the vicinity of the infected cell (Experimental Procedures) but, separated by a gap, did not exhibit markedly more IL-8 than class 3 cells distant from any infection foci (Figure 6F). Collectively, these results demonstrated that the expression of IL-8 in bystander cells depends on cell-cell contact and is most probably not mediated by paracrine signaling.

Cell-Cell Propagation of Inflammatory Signals Is Mediated by Connexin Gap Junctions

An alternative hypothesis to paracrine signaling is direct communication via gap junction channels formed by connexin proteins. This hypothesis was directly tested by evaluating the effect of the gap junction blocker 18β-glycyrrhetinic acid (18β-GA) on IL-8 expression in bystander cells during *S. flexneri* infection of Caco-2 cells. In conditions of drug treatment that blocked Lucifer Yellow transfer through gap junctions of adjacent Caco-2 cells (Figure S7A), IL-8 expression in bystander

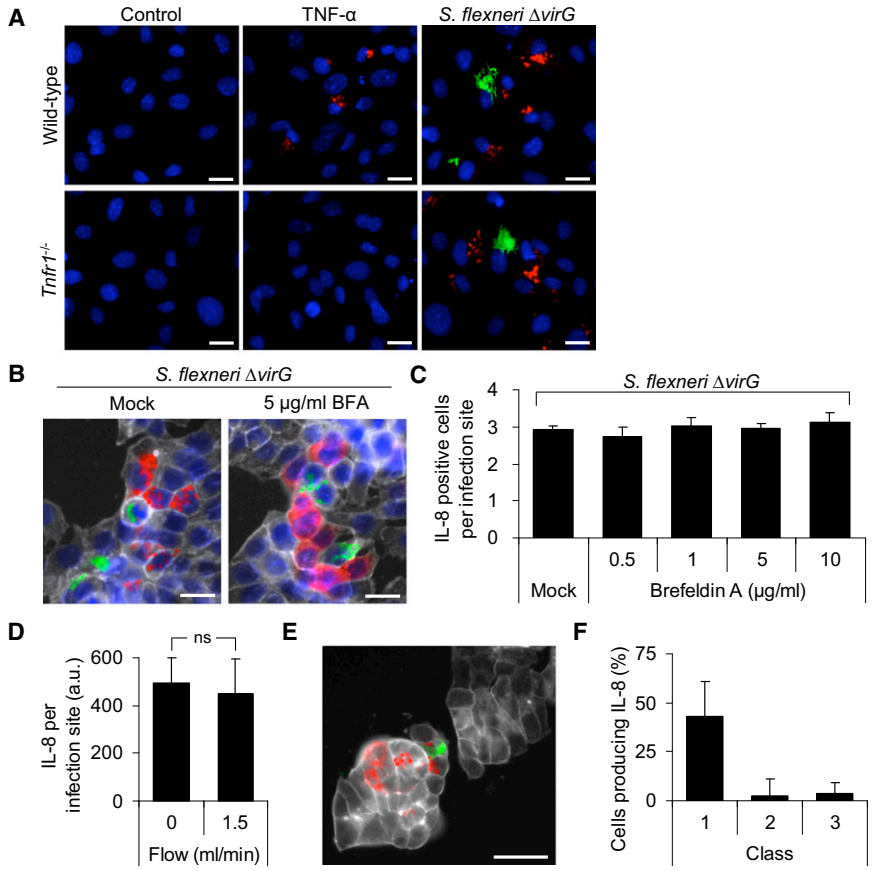

Figure 6. Bystander Activation Is Not Mediated by Paracrine Signaling but Is Cell-Cell Contact Dependent

(A) MIP-2 expression in wild-type and *Tnfr1*$^{-/-}$ MEF cells after TNF-α stimulation or *S. flexneri* infection visualized by fluorescence microscopy. After infection, cells were stained for MIP-2 and DNA with a MIP-2 antibody and Hoechst, respectively (MIP-2 in red, *S. flexneri* in green, Hoechst in blue). Scale bars represent 20 μm.

(B) Bystander IL-8 expression in Caco-2 cells pretreated with BFA and infected with *S. flexneri*. After infection (*S. flexneri* in green), cells were stained for IL-8, DNA, and F-actin with an IL-8 antibody (in red), Hoechst (in blue), and phalloidin (in gray), respectively. Scale bars represent 20 μm.

(C) Quantification of bystander IL-8 expression upon BFA treatment by automated image analysis (means ± SD of triplicate wells, graph representative of two independent experiments).

(D) Quantification of bystander IL-8 expression under flow conditions. IL-8 was quantified by measuring for each infected cell the area of IL-8 staining (a.u., arbitrary units, means ± SD, n = 10, graph representative of two independent experiments).

(E) Cell-cell contact analysis of bystander IL-8 expression. Caco-2 cells, seeded at subconfluent density and infected with *S. flexneri* (in green), were stained for IL-8 (in red) and F-actin (in gray). Scale bar represents 50 μm.

(F) Fractions of IL-8-producing cells in class 1, 2, 3 cell populations as defined in Experimental Procedures (means ± SD, n > 38, graph representative of two independent experiments).

cells of infection was strongly reduced (Figures 7A and 7B). In contrast, TNF-α-induced IL-8 secretion, used as control, was not affected (Figures S7B and S7C). A similar result was obtained with the gap junction inhibitor carbenoxolone (Figures S7D and S7E). Furthermore, treatment with glycyrrhizic acid, a compound structurally related to 18β-GA but which fails to block gap junction communication at concentrations below 100 μM (Davidson et al., 1986), had no effect on *S. flexneri*-induced IL-8 expression by bystander cells (Figure 7B). Taken together, these results suggested that IL-8 expression by bystander cells of infection was mediated by communication through gap junctions.

Because gap junction inhibitors have unspecific effects, we further validated this finding by testing whether the propagation of inflammatory signals was connexin dependent. In A431 cells that are poorly coupled via gap junctions and express connexin43 (Cx43) below the level of detection with antibodies (Troyanovsky et al., 1994), very limited activation of NF-κB, JNK, p38, and ERK and residual IL-8 expression were found in bystander cells of *S. flexneri* infection (Figure 7C, left, and Figure 7D, top). In contrast, in Cx43-overexpressing A431 cells (A431-Cx43) that are effectively coupled via gap junctions (Neijssen et al., 2005), large foci of NF-κB, JNK, p38, and ERK activation and IL-8 expression were found around infected cells (Figure 7C, right, and Figure 7D, bottom). Quantification of IL-8 expression in consecutive A431 or A431-Cx43 bystander cells by automated image processing, as described in Supplemental Experimental Procedures, confirmed that the propagation of IL-8 expression was Cx43 dependent (Figures 7D and 7E). As expected, bystander IL-8 expression was strongly reduced when A431-Cx43 cells were depleted of Cx43 by RNA interference (Figure 7F and Figure S7F) or treated with 18β-GA (Figure 7G and Figure S7G).

In contrast to typical hemichannel-based signaling, communication via gap junction channels requires connexin proteins in both donor and recipient cells. To confirm that this condition was fulfilled for bystander activation, the propagation of inflammatory signals from *S. flexneri*-infected A431-Cx43 cells to either A431-Cx43 or A431 bystander cells was analyzed in experiments where A431-Cx43 and A431 cells were mixed prior seeding. Cx43, used to discriminate A431 and A431-Cx43 cells, as well as IL-8 were detected by immunofluorescence. Whereas IL-8 expression robustly spread within consecutive A431-Cx43 cells, the propagation from infected A431-Cx43 to adjacent A431 cells was very limited (Figure S7H). This observation, quantified by automated image processing (Figure 7H and Figure S7I), indicated that Cx43 proteins were also required in uninfected bystander cells to efficiently potentiate inflammation. Taken together, these data convincingly showed that the propagation of inflammation during bacterial infection of epithelial cells depends on connexin gap junctions.

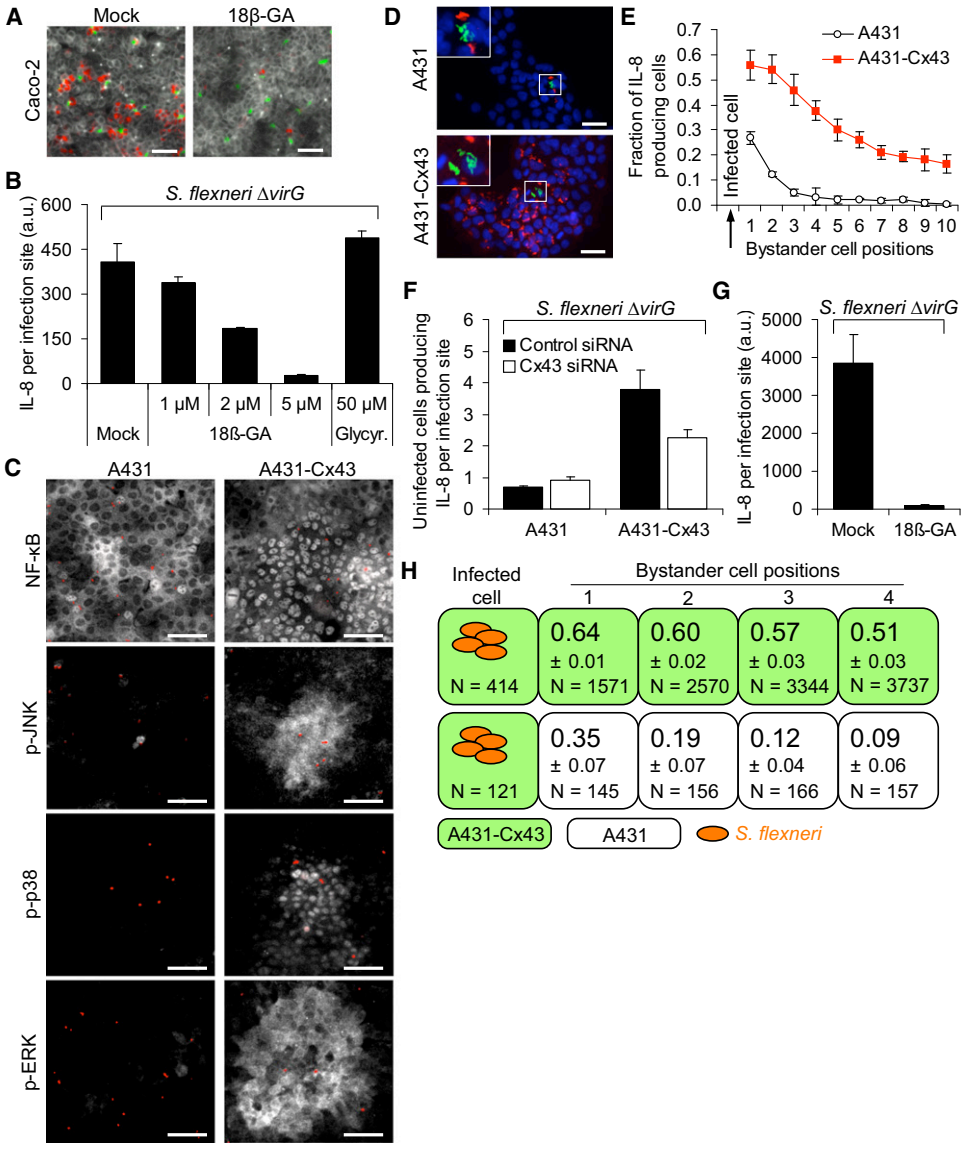

Figure 7. Propagation of Inflammation Is Mediated by Gap Junctions

(A) Effect of 18β-GA on IL-8 expression during infection of Caco-2 cells. Cells were pretreated with 18β-GA, infected with Δ*virG S. flexneri*, and stained for IL-8 and F-actin with an IL-8 antibody and phalloidin, respectively (IL-8 in red, *S. flexneri* in green, F-actin in gray). Scale bars represent 50 μm.

(B) Quantification of IL-8 accumulation per site of infection in cells left untreated or pretreated with 18β-GA or glycyrrhizine. Quantification was performed by automated image processing as described in Supplemental Experimental Procedures (means ± SD of triplicate wells, graph representative of two independent experiments).

(C) Cell-cell propagation of proinflammatory signals in A431 and A431-Cx43 cells visualized by immunofluorescence. NF-κB p65, p-JNK, p-p38, and p-ERK immunofluorescence staining in A431 cells (left) and A431-Cx43 cells (right) after *S. flexneri* infection (NF-κB p65, p-JNK, p-p38, and p-ERK in gray, *S. flexneri* in red). Scale bars represent 40 μm.

(D) Propagation of IL-8 expression during *S. flexneri* infection of A431 and A431-Cx43 cells visualized by immunofluorescence. After infection, cells were stained for IL-8 and DNA with an IL-8 antibody and Hoechst, respectively (IL-8 in red, *S. flexneri* in green, Hoechst in blue). Inserts show the infection foci (magnification: ×2.5). Scale bars represent 40 μm.

(E) Spatial propagation of IL-8 expression in consecutive A431 or A431-Cx43 bystander cells during *S. flexneri* infection (means ± SD of six wells; graph representative of two independent experiments). Quantification was performed as described in Supplemental Experimental Procedures.

(F) Quantification of bystander IL-8 expression after siRNA-mediated Cx43 depletion. IL-8 was analyzed by immunofluorescence in A431 and A431-Cx43 cells transfected with control or Cx43 siRNAs and infected with *S. flexneri* and quantified by automated image analysis (means ± SD of triplicate wells, graph representative of two independent experiments, p = 3.9E-06).

(G) Quantification of bystander IL-8 expression in A431-Cx43 cells pretreated with 18β-GA and infected with *S. flexneri* (means ± SD of triplicate wells, graph representative of three independent experiments).

(H) Spatial propagation of IL-8 expression from *S. flexneri*-infected A431-Cx43 cells into either A431-Cx43 or A431 adjacent cells. Each number corresponds to the fraction of IL-8-producing cells for a given bystander cell position. Quantification was performed by automated image processing and is described in Supplemental Experimental Procedures (means ± SD of triplicate wells, graph representative of two independent experiments, p < 7.5E-04 at any given position).

DISCUSSION

In the present study, we provide evidence that during *S. flexneri* infection, the activation of the proinflammatory pathways NF-κB, JNK, ERK, and p38 propagates from infected to uninfected adjacent cells leading to IL-8 expression in bystander cells of infection. This mechanism, mediated by gap junction communication between infected and uninfected cells, circumvents the immunosuppressive activity of bacterial effectors and massively amplifies inflammation during bacterial infection.

Nod1 contributes to the detection of intracellular *S. flexneri* via the recognition of peptidoglycan-derived peptides (Girardin et al., 2003). In infected IECs, Nod1 ligation leads to NF-κB activation and upregulation of proinflammatory genes. By using an in vitro single-cell assay of *S. flexneri* infection, we found that NF-κB activation was not restricted to infected cells. Indeed, by performing infections at low MOIs, we observed within minutes of infection the propagation of NF-κB activation from infected to uninfected bystander cells. This cell-cell communication mechanism resulted in massive amplification of the total NF-κB response to *S. flexneri* infection. Because NF-κB controls the expression of proinflammatory genes, this result suggested that the mechanism of bystander activation may amplify the inflammatory response of an infected epithelial cell layer. This hypothesis was supported by the observation that JNK, ERK, and p38, three kinases involved in the control of inflammation, were also activated in bystander cells of *S. flexneri* infection. Noticeably, p38 activation was markedly higher in bystander than infected cells, suggesting that the effector OspF, which dephosphorylates p38 in the nucleus of infected cells via its phosphothreonine-lyase activity, did not affect p38 bystander activation. This hypothesis was validated by the observation that the deletion of *ospF* enhanced p38 activation in infected but not in bystander cells. Infection at low MOI reflects the early phase of Shigellosis, when the number of bacteria that have reached the basolateral surface of the IECs is limited. By rapidly propagating NF-κB and MAP kinase activation to uninfected cells, the mechanism of bystander activation may enable the host to fully activate these signaling pathways before their manipulation by future internalized bacteria, for instance via the effectors OspG and OspF (Arbibe et al., 2007; Kim et al., 2005).

The concept of bystander responses has been previously described in the context of ionizing radiation where nonirradiated cells receive signals from neighboring or distant irradiated ones (Hamada et al., 2007), in wound healing (Yang et al., 2004), or more recently after double-stranded DNA recognition (Patel et al., 2009). In all cases, the activation of signaling pathways emanates from cells exposed to local stress and propagates into the adjacent healthy tissue to amplify and orchestrate a multicellular response to an aggression. Here, we provide evidence for a similar mechanism in innate immunity against pathogenic bacteria.

By attracting neutrophils to the infected area, IL-8 has a central function in innate immunity against pathogens and in Shigellosis, in particular. It has been proposed that IL-8 is secreted by *S. flexneri*-infected cells after recognition of intracellular peptidoglycan-derived peptides via Nod1 (Girardin et al., 2003). Yet, the immunosuppressive activity of several effectors that alters signaling in infected cells challenges the ability of these cells to secrete large amounts of IL-8 as observed in Shigellosis. To directly address this question, we analyzed IL-8 expression during *S. flexneri* infection at the mRNA and protein level by in situ hybridization and intracellular immunofluorescence microscopy, respectively, two methods that combine single-cell resolution and spatial information at the site of infection. Here, we showed that the propagation of NF-κB, JNK, ERK, and p38 activation leads to IL-8 expression in bystander cells of infection. This mechanism efficiently amplifies the total IL-8 response of the infected cell monolayer by increasing the number of IL-8-producing cells per site of infection. Furthermore, our results clearly demonstrated that infected cells were inefficient at producing IL-8, confirming the immunosuppressive activities of secreted effectors on IL-8 expression. In line with the effect of OspF on p38 and histone H3 phosphorylation, IL-8 production was increased in cells infected with a Δ*ospF* mutant. However, the deletion of *ospF* had only a limited effect on IL-8 expression, suggesting that the complete block observed in infected cells is mediated by multiple effectors. Additional effectors such as OspG, OspB, and $IpaH_{9.8}$ may also contribute to block IL-8 expression in infected cells (Kim et al., 2005; Okuda et al., 2005; Zurawski et al., 2009). Interestingly, we showed that OspF did not affect IL-8 expression in bystander cells, indicating that through cell-cell communication, the host appears to circumvent the activity of OspF in infected cells and amplifies the global IL-8 response to *S. flexneri* infection. In the rabbit intestinal loop model of Shigellosis, IL-8 expression was found in epithelial cells located beyond the zones of bacterial invasion, providing evidence for the physiological relevance of bystander IL-8 expression in vivo (Sansonetti et al., 1999).

IL-8 expression was also found in bystander cells of *S. typhimurium* and *L. monocytogenes* infection, showing that the potentiation of innate immunity by cell-cell communication corresponded to a broad host response to bacterial infection. However, the contribution of this mechanism to inflammation can vary for different pathogens. It depends on its frequency of occurrence but also on the ability of bacteria to alter signaling in infected cells. For *S. flexneri* that very efficiently blocks signaling in infected cells, bystander activation clearly constitutes the key pathway of IL-8 expression.

We addressed the role of peptidoglycan recognition in the mechanism of cell-cell communication leading to IL-8 expression in bystander cells and its underlying molecular basis. Interestingly, we found that the microinjection of the Nod1 ligand TriDAP was sufficient to induce IL-8 expression in bystander cells of microinjection, suggesting that the recognition of Nod1 ligands in infected cells may be sufficient to generate the underlying signals that mediate IL-8 expression in bystander cells of *S. flexneri* infection. Cell-cell communication can be mediated by different mechanisms: paracrine signaling, direct diffusion of small molecules through gap junctions, or membrane protein interactions. In Caco-2 cells, bystander IL-8 expression was not inhibited by BFA treatment or by perfusion, indicating that this process was most probably not mediated by paracrine signaling. Furthermore, it was cell-cell contact dependent, and therefore compatible with gap junction-mediated communication that enables direct diffusion of small molecules between adjacent

cells. This hypothesis was confirmed by showing that the mechanism of bystander IL-8 expression was blocked by gap junction inhibitors, limited in cells that are poorly coupled via gap junctions, and massively amplified by the overexpression of the gap junction protein Cx43. Finally, as required for the formation of connexins gap junction channels between adjacent cells, we showed that the presence of connexin proteins was necessary in both infected and bystander cells to efficiently propagate inflammation during bacterial infection.

Further studies are required to identify the small molecules (i.e., <2 kDa) diffusing from infected to bystander cells that control NF-κB, JNK, ERK, and p38 activation and lead to IL-8 expression during *S. flexneri* infection. Among potential candidates, the roles of known second messengers, which are involved in proinflammatory gene expression, including calcium, IP3, and cAMP, should be examined. An alternative hypothesis is the direct diffusion of small peptidoglycan-derived peptides through gap junctions.

In summary, we show that during *S. flexneri* infection, the activation of the proinflammatory pathways NF-κB, JNK, ERK, and p38 propagates from infected to uninfected adjacent cells leading to IL-8 expression in bystander cells of infection. This mechanism enables the host to circumvent the immunosuppressive activity of bacterial effectors and to massively amplify inflammation during bacterial infection. Moreover, by showing that this process is gap junction mediated, we provide evidence for a direct connection between gap junction communication and amplification of innate immunity during bacterial infection.

EXPERIMENTAL PROCEDURES

Cell Culture

HeLa, A549, Caco-2, A431, and MEF cells were cultured in Dulbecco's modified Eagle's medium (DMEM) supplemented with 10% FCS and 2 mM L-Glutamine. HUVECs were generously provided by C. Dehio (Biozentrum, University of Basel, Switzerland) and cultivated as previously described (Dehio et al., 1997).

Bacterial Strains

The *S. flexneri* strains M90T wild-type, its noninvasive derivative BS176, and the *icsA (virG)* deletion mutant were generously provided by P. Sansonetti (Bernardini et al., 1989). The Δ*virG* Δ*ospF* deletion mutant was generated as described in Supplemental Experimental Procedures (Table S1). The *Salmonella typhimurium* LT2 strain was provided by U. Jenal (Biozentrum, University of Basel, Switzerland) and the stably expressing GFP *Listeria monocytogenes* A21/B5 strain by M. Loessner (ETH Zurich, Switzerland).

Infection Assays

S. flexneri, S. typhimurium, and *L. monocytognes* were used in exponential growth phase. *S. flexneri* and *S. typhimurium* were coated with poly-L-lysine prior to infection. Cells seeded in 96-well plates were infected at indicated MOIs in DMEM supplemented with 10 mM HEPES and 2 mM L-glutamine. After adding bacteria, plates were centrifuged for 5 min and placed at 37°C for indicated time periods. Extracellular bacteria were killed by gentamicin (100 μg ml^{-1}). Infection assays were stopped by 4% PFA fixation.

Immunofluorescence and IL-8 Measurements

Immunofluorescence and IL-8 measurements were performed as described in Supplemental Experimental Procedures.

Automated Microscopy and Image Analysis

Images were automatically acquired with an ImageXpress Micro (Molecular devices, Sunnyvale, USA). Image analysis was performed via CellProfiler (Carpenter et al., 2006) and MATLAB (The MathWorks, Inc, Natick, USA) as described in Supplemental Experimental Procedures.

Microinjection and Flow Chamber Experiments

Microinjection and flow chamber experiments are described in Supplemental Experimental Procedures.

Analysis of Cell-Cell Contact

Infection was performed at subconfluent cell density. Cellular contacts and IL-8 were visualized by phalloidin and IL-8 staining, respectively. For each site of infection, the distance between the infected cell and the most distant bystander cell producing IL-8 was used as the radius of the "circle of bystander activation" centered on the infected cell. Within this circle, cells contacting directly the infected cell or indirectly by interacting with other bystander cells were classified as class 1. Cells making no direct or indirect contact with infected cells were defined as class 2. Cells located outside the circle and distant from any sites of infection were defined as class 3.

Statistical Analysis

Data are expressed as mean ± standard deviation of triplicate samples. p values were calculated with a two-tailed two-sample equal variance t test.

SUPPLEMENTAL INFORMATION

Supplemental Information includes Supplemental Experimental Procedures, seven figures, and one table and can be found with this article online at doi:10.1016/j.immuni.2010.10.015.

ACKNOWLEDGMENTS

We thank J. Neefjes (NKI, Amsterdam, Netherlands) and M. Kelliher (Massachusetts Medical School, Worcester, USA) for the generous gift of A431-Cx43 cells and *Tnfr1*$^{-/-}$ MEFs, respectively. We also thank G. Cornelis, U. Jenal, and C. Dehio for comments on the manuscript and M. Podvinec for help with research IT. This work was funded by the Swiss National Science Foundation (grant 3100A0-113561 to C.A.) and the InfectX project from SystemsX.ch. C.A.K. was supported by the Werner-Siemens Foundation.

Received: May 10, 2010
Revised: August 25, 2010
Accepted: September 17, 2010
Published online: November 18, 2010

REFERENCES

Arbibe, L., Kim, D.W., Batsche, E., Pedron, T., Mateescu, B., Muchardt, C., Parsot, C., and Sansonetti, P.J. (2007). An injected bacterial effector targets chromatin access for transcription factor NF-kappaB to alter transcription of host genes involved in immune responses. Nat. Immunol. *8*, 47–56.

Bernardini, M.L., Mounier, J., d'Hauteville, H., Coquis-Rondon, M., and Sansonetti, P.J. (1989). Identification of icsA, a plasmid locus of Shigella flexneri that governs bacterial intra- and intercellular spread through interaction with F-actin. Proc. Natl. Acad. Sci. USA *86*, 3867–3871.

Carpenter, A.E., Jones, T.R., Lamprecht, M.R., Clarke, C., Kang, I.H., Friman, O., Guertin, D.A., Chang, J.H., Lindquist, R.A., Moffat, J., et al. (2006). CellProfiler: Image analysis software for identifying and quantifying cell phenotypes. Genome Biol. *7*, R100.

Cornelis, G.R. (2006). The type III secretion injectisome. Nat. Rev. Microbiol. *4*, 811–825.

Davidson, J.S., Baumgarten, I.M., and Harley, E.H. (1986). Reversible inhibition of intercellular junctional communication by glycyrrhetinic acid. Biochem. Biophys. Res. Commun. *134*, 29–36.

Dehio, C., Meyer, M., Berger, J., Schwarz, H., and Lanz, C. (1997). Interaction of *Bartonella henselae* with endothelial cells results in bacterial aggregation on the cell surface and the subsequent engulfment and internalisation of the bacterial aggregate by a unique structure, the invasome. J. Cell Sci. *110*, 2141–2154.

Dong, C., Davis, R.J., and Flavell, R.A. (2002). MAP kinases in the immune response. Annu. Rev. Immunol. *20*, 55–72.

Eckmann, L., Kagnoff, M.F., and Fierer, J. (1993). Epithelial cells secrete the chemokine interleukin-8 in response to bacterial entry. Infect. Immun. *61*, 4569–4574.

Girardin, S.E., Boneca, I.G., Carneiro, L.A., Antignac, A., Jéhanno, M., Viala, J., Tedin, K., Taha, M.K., Labigne, A., Zähringer, U., et al. (2003). Nod1 detects a unique muropeptide from gram-negative bacterial peptidoglycan. Science *300*, 1584–1587.

Hamada, N., Matsumoto, H., Hara, T., and Kobayashi, Y. (2007). Intercellular and intracellular signaling pathways mediating ionizing radiation-induced bystander effects. J. Radiat. Res. (Tokyo) *48*, 87–95.

Holtmann, H., Winzen, R., Holland, P., Eickemeier, S., Hoffmann, E., Wallach, D., Malinin, N.L., Cooper, J.A., Resch, K., and Kracht, M. (1999). Induction of interleukin-8 synthesis integrates effects on transcription and mRNA degradation from at least three different cytokine- or stress-activated signal transduction pathways. Mol. Cell. Biol. *19*, 6742–6753.

Islam, D., Veress, B., Bardhan, P.K., Lindberg, A.A., and Christensson, B. (1997). In situ characterization of inflammatory responses in the rectal mucosae of patients with shigellosis. Infect. Immun. *65*, 739–749.

Iwai, H., Kim, M., Yoshikawa, Y., Ashida, H., Ogawa, M., Fujita, Y., Muller, D., Kirikae, T., Jackson, P.K., Kotani, S., and Sasakawa, C. (2007). A bacterial effector targets Mad2L2, an APC inhibitor, to modulate host cell cycling. Cell *130*, 611–623.

Kim, D.W., Lenzen, G., Page, A.L., Legrain, P., Sansonetti, P.J., and Parsot, C. (2005). The *Shigella flexneri* effector OspG interferes with innate immune responses by targeting ubiquitin-conjugating enzymes. Proc. Natl. Acad. Sci. USA *102*, 14046–14051.

Köhler, H., Rodrigues, S.P., and McCormick, B.A. (2002). *Shigella flexneri* interactions with the basolateral membrane domain of polarized model intestinal epithelium: Role of lipopolysaccharide in cell invasion and in activation of the mitogen-activated protein kinase ERK. Infect. Immun. *70*, 1150–1158.

Kufer, T.A., Banks, D.J., and Philpott, D.J. (2006). Innate immune sensing of microbes by Nod proteins. Ann. N Y Acad. Sci. *1072*, 19–27.

Lee, J., Mira-Arbibe, L., and Ulevitch, R.J. (2000). TAK1 regulates multiple protein kinase cascades activated by bacterial lipopolysaccharide. J. Leukoc. Biol. *68*, 909–915.

Li, H., Xu, H., Zhou, Y., Zhang, J., Long, C., Li, S., Chen, S., Zhou, J.M., and Shao, F. (2007). The phosphothreonine lyase activity of a bacterial type III effector family. Science *315*, 1000–1003.

Makino, S., Sasakawa, C., Kamata, K., Kurata, T., and Yoshikawa, M. (1986). A genetic determinant required for continuous reinfection of adjacent cells on large plasmid in *S. flexneri* 2a. Cell *46*, 551–555.

Mollenhauer, H.H., Morré, D.J., and Rowe, L.D. (1990). Alteration of intracellular traffic by monensin; Mechanism, specificity and relationship to toxicity. Biochim. Biophys. Acta *1031*, 225–246.

Neijssen, J., Herberts, C., Drijfhout, J.W., Reits, E., Janssen, L., and Neefjes, J. (2005). Cross-presentation by intercellular peptide transfer through gap junctions. Nature *434*, 83–88.

Ninomiya-Tsuji, J., Kishimoto, K., Hiyama, A., Inoue, J., Cao, Z., and Matsumoto, K. (1999). The kinase TAK1 can activate the NIK-I kappaB as well as the MAP kinase cascade in the IL-1 signalling pathway. Nature *398*, 252–256.

Okuda, J., Toyotome, T., Kataoka, N., Ohno, M., Abe, H., Shimura, Y., Seyedarabi, A., Pickersgill, R., and Sasakawa, C. (2005). *Shigella* effector IpaH9.8 binds to a splicing factor U2AF(35) to modulate host immune responses. Biochem. Biophys. Res. Commun. *333*, 531–539.

Parsot, C. (2009). *Shigella* type III secretion effectors: How, where, when, for what purposes? Curr. Opin. Microbiol. *12*, 110–116.

Patel, S.J., King, K.R., Casali, M., and Yarmush, M.L. (2009). DNA-triggered innate immune responses are propagated by gap junction communication. Proc. Natl. Acad. Sci. USA *106*, 12867–12872.

Pédron, T., Thibault, C., and Sansonetti, P.J. (2003). The invasive phenotype of *Shigella flexneri* directs a distinct gene expression pattern in the human intestinal epithelial cell line Caco-2. J. Biol. Chem. *278*, 33878–33886.

Phalipon, A., and Sansonetti, P.J. (2007). *Shigella's* ways of manipulating the host intestinal innate and adaptive immune system: A tool box for survival? Immunol. Cell Biol. *85*, 119–129.

Saccani, S., Pantano, S., and Natoli, G. (2002). p38-dependent marking of inflammatory genes for increased NF-kappa B recruitment. Nat. Immunol. *3*, 69–75.

Sansonetti, P.J., Arondel, J., Huerre, M., Harada, A., and Matsushima, K. (1999). Interleukin-8 controls bacterial transepithelial translocation at the cost of epithelial destruction in experimental shigellosis. Infect. Immun. *67*, 1471–1480.

Schroeder, G.N., and Hilbi, H. (2008). Molecular pathogenesis of *Shigella* spp.: Controlling host cell signaling, invasion, and death by type III secretion. Clin. Microbiol. Rev. *21*, 134–156.

Strober, W., Murray, P.J., Kitani, A., and Watanabe, T. (2006). Signalling pathways and molecular interactions of NOD1 and NOD2. Nat. Rev. Immunol. *6*, 9–20.

Troyanovsky, S.M., Troyanovsky, R.B., Eshkind, L.G., Krutovskikh, V.A., Leube, R.E., and Franke, W.W. (1994). Identification of the plakoglobin-binding domain in desmoglein and its role in plaque assembly and intermediate filament anchorage. J. Cell Biol. *127*, 151–160.

Wang, C., Deng, L., Hong, M., Akkaraju, G.R., Inoue, J., and Chen, Z.J. (2001). TAK1 is a ubiquitin-dependent kinase of MKK and IKK. Nature *412*, 346–351.

Yang, L., Cranson, D., and Trinkaus-Randall, V. (2004). Cellular injury induces activation of MAPK via P2Y receptors. J. Cell. Biochem. *91*, 938–950.

Zurawski, D.V., Mumy, K.L., Faherty, C.S., McCormick, B.A., and Maurelli, A.T. (2009). *Shigella flexneri* type III secretion system effectors OspB and OspF target the nucleus to downregulate the host inflammatory response via interactions with retinoblastoma protein. Mol. Microbiol. *71*, 350–368.